Measurement of ϒ(1S + 2S + 3S) production in p + p and Au + Au collisions at √sNN = 200 GeV

(PHENIX Collaboration) Adare, A.; ...; Makek, Mihael; ...; Zolin, L.

Measurement of $\Upsilon(1S+2S+3S)$ production in $p+p$ and Au + Au collisions at $\sqrt{s_{NN}} = 200$ GeV

A. Adare,[14] S. Afanasiev,[32] C. Aidala,[41,45,46] N. N. Ajitanand,[65] Y. Akiba,[59,60] R. Akimoto,[13] H. Al-Bataineh,[53] H. Al-Ta'ani,[53] J. Alexander,[65] A. Angerami,[15] K. Aoki,[37,59] N. Apadula,[66] L. Aphecetche,[67] Y. Aramaki,[13,59] J. Asai,[59] H. Asano,[37,59] E. C. Aschenauer,[8] E. T. Atomssa,[38,66] R. Averbeck,[66] T. C. Awes,[55] B. Azmoun,[8] V. Babintsev,[26] M. Bai,[7] G. Baksay,[21] L. Baksay,[21] A. Baldisseri,[17] B. Bannier,[66] K. N. Barish,[9] P. D. Barnes,[41,*] B. Bassalleck,[52] A. T. Basye,[1] S. Bathe,[6,9,60] S. Batsouli,[55] V. Baublis,[58] C. Baumann,[47] S. Baumgart,[59] A. Bazilevsky,[8] S. Belikov,[8,*] R. Belmont,[71] R. Bennett,[66] A. Berdnikov,[62] Y. Berdnikov,[62] A. A. Bickley,[14] X. Bing,[54] D. S. Blau,[36] J. G. Boissevain,[41] J. S. Bok,[53] H. Borel,[17] K. Boyle,[60,66] M. L. Brooks,[41] H. Buesching,[8] V. Bumazhnov,[26] G. Bunce,[8,60] S. Butsyk,[41,52] C. M. Camacho,[41] S. Campbell,[66] P. Castera,[66] B. S. Chang,[75] W. C. Chang,[2] J.-L. Charvet,[17] C.-H. Chen,[66] S. Chernichenko,[26] C. Y. Chi,[15] M. Chiu,[8,27] I. J. Choi,[27,75] J. B. Choi,[11] S. Choi,[64] R. K. Choudhury,[5] P. Christiansen,[43] T. Chujo,[70] P. Chung,[65] A. Churyn,[26] O. Chvala,[9] V. Cianciolo,[55] Z. Citron,[66] B. A. Cole,[15] M. Connors,[66] P. Constantin,[41] M. Csanád,[19] T. Csörgő,[74] T. Dahms,[66] S. Dairaku,[37,59] K. Das,[22] A. Datta,[45] M. S. Daugherity,[1] G. David,[8] A. Denisov,[26] D. d'Enterria,[38] A. Deshpande,[60,66] E. J. Desmond,[8] K. V. Dharmawardane,[53] O. Dietzsch,[63] L. Ding,[30] A. Dion,[30,66] M. Donadelli,[63] O. Drapier,[38] A. Drees,[66] K. A. Drees,[7] A. K. Dubey,[73] J. M. Durham,[41,66] A. Durum,[26] D. Dutta,[5] V. Dzhordzhadze,[9] L. D'Orazio,[44] S. Edwards,[7] Y. V. Efremenko,[55] F. Ellinghaus,[14] T. Engelmore,[15] A. Enokizono,[40,55] H. En'yo,[59,60] S. Esumi,[70] K. O. Eyser,[9] B. Fadem,[48] D. E. Fields,[52,60] M. Finger,[10] M. Finger Jr.,[10] F. Fleuret,[38] S. L. Fokin,[36] Z. Fraenkel,[73,*] J. E. Frantz,[54,66] A. Franz,[8] A. D. Frawley,[22] K. Fujiwara,[59] Y. Fukao,[37,59] T. Fusayasu,[50] K. Gainey,[1] C. Gal,[66] A. Garishvili,[68] I. Garishvili,[40,68] A. Glenn,[14,40] H. Gong,[66] X. Gong,[65] M. Gonin,[38] J. Gosset,[17] Y. Goto,[59,60] R. Granier de Cassagnac,[38] N. Grau,[3,15] S. V. Greene,[71] M. Grosse Perdekamp,[27,60] T. Gunji,[13] L. Guo,[41] H.-Å. Gustafsson,[43,*] T. Hachiya,[59] A. Hadj Henni,[67] J. S. Haggerty,[8] K. I. Hahn,[20] H. Hamagaki,[13] R. Han,[57] J. Hanks,[15] E. P. Hartouni,[40] K. Haruna,[25] K. Hashimoto,[59,61] E. Haslum,[43] R. Hayano,[13] X. He,[23] M. Heffner,[40] T. K. Hemmick,[66] T. Hester,[9] J. C. Hill,[30] M. Hohlmann,[21] R. S. Hollis,[9] W. Holzmann,[65] K. Homma,[25] B. Hong,[35] T. Horaguchi,[13,59,69,70] Y. Hori,[13] D. Hornback,[68] S. Huang,[71] T. Ichihara,[59,60] R. Ichimiya,[59] H. Iinuma,[34,37,59] Y. Ikeda,[59,70] K. Imai,[31,37,59] J. Imrek,[18] M. Inaba,[70] A. Iordanova,[9] D. Isenhower,[1] M. Ishihara,[59] T. Isobe,[13,59] M. Issah,[65,71] A. Isupov,[32] D. Ivanischev,[58] D. Ivanishchev,[58] B. V. Jacak,[66] M. Javani,[23] J. Jia,[8,15,65] X. Jiang,[41] J. Jin,[15] B. M. Johnson,[8] K. S. Joo,[49] D. Jouan,[56] D. S. Jumper,[27] F. Kajihara,[13] S. Kametani,[59] N. Kamihara,[60] J. Kamin,[66] S. Kaneti,[66] B. H. Kang,[24] J. H. Kang,[75] J. S. Kang,[24] J. Kapustinsky,[41] K. Karatsu,[37,59] M. Kasai,[59,61] D. Kawall,[45,60] A. V. Kazantsev,[36] T. Kempel,[30] A. Khanzadeev,[58] K. M. Kijima,[25] J. Kikuchi,[72] B. I. Kim,[35] C. Kim,[35] D. H. Kim,[49] D. J. Kim,[33,75] E. Kim,[64] E.-J. Kim,[11] H. J. Kim,[75] K.-B. Kim,[11] S. H. Kim,[75] Y.-J. Kim,[27] Y. K. Kim,[24] E. Kinney,[14] K. Kiriluk,[14] Á. Kiss,[19] E. Kistenev,[8] J. Klatsky,[22] J. Klay,[40] C. Klein-Boesing,[47] D. Kleinjan,[9] P. Kline,[66] L. Kochenda,[58] Y. Komatsu,[13] B. Komkov,[58] M. Konno,[70] J. Koster,[27] D. Kotchetkov,[54] D. Kotov,[58,62] A. Kozlov,[73] A. Král,[16] A. Kravitz,[15] F. Krizek,[33] G. J. Kunde,[41] K. Kurita,[59,61] M. Kurosawa,[59] M. J. Kweon,[35] Y. Kwon,[68,75] G. S. Kyle,[53] R. Lacey,[65] Y. S. Lai,[15] J. G. Lajoie,[30] D. Layton,[27] A. Lebedev,[30] B. Lee,[24] D. M. Lee,[41] J. Lee,[20] K. B. Lee,[35] K. S. Lee,[35] S. H. Lee,[66] S. R. Lee,[11] T. Lee,[64] M. J. Leitch,[41] M. A. L. Leite,[63] M. Leitgab,[27] B. Lenzi,[63] B. Lewis,[66] X. Li,[12] P. Liebing,[60] S. H. Lim,[75] L. A. Linden Levy,[14] T. Liška,[16] A. Litvinenko,[32] H. Liu,[53] M. X. Liu,[41] B. Love,[71] D. Lynch,[8] C. F. Maguire,[71] Y. I. Makdisi,[7] M. Makek,[73,76] A. Malakhov,[32] M. D. Malik,[52] A. Manion,[66] V. I. Manko,[36] E. Mannel,[15] Y. Mao,[57,59] L. Mašek,[10,29] H. Masui,[70] S. Masumoto,[13] F. Matathias,[15] M. McCumber,[14,66] P. L. McGaughey,[41] D. McGlinchey,[14,22] C. McKinney,[27] N. Means,[66] M. Mendoza,[9] B. Meredith,[27] Y. Miake,[70] T. Mibe,[34] A. C. Mignerey,[44] P. Mikeš,[29] K. Miki,[70] A. Milov,[8,73] D. K. Mishra,[5] M. Mishra,[4] J. T. Mitchell,[8] Y. Miyachi,[59,69] S. Miyasaka,[59,69] A. K. Mohanty,[5] H. J. Moon,[49] Y. Morino,[13] A. Morreale,[9] D. P. Morrison,[8,†] S. Motschwiller,[48] T. V. Moukhanova,[36] D. Mukhopadhyay,[71] T. Murakami,[37,59] J. Murata,[59,61] T. Nagae,[37] S. Nagamiya,[34,59] J. L. Nagle,[14,‡] M. Naglis,[73] M. I. Nagy,[19,74] I. Nakagawa,[59,60] Y. Nakamiya,[25] K. R. Nakamura,[37,59] T. Nakamura,[25,59] K. Nakano,[59,69] C. Nattrass,[68] A. Nederlof,[48] J. Newby,[40] M. Nguyen,[66] M. Nihashi,[25,59] T. Niida,[70] R. Nouicer,[8,60] N. Novitzky,[33] A. S. Nyanin,[36] E. O'Brien,[8] S. X. Oda,[13] C. A. Ogilvie,[30] M. Oka,[70] K. Okada,[60] Y. Onuki,[59] A. Oskarsson,[43] M. Ouchida,[25,59] K. Ozawa,[13] R. Pak,[8] A. P. T. Palounek,[41] V. Pantuev,[28,66] V. Papavassiliou,[53] B. H. Park,[24] I. H. Park,[20] J. Park,[64] S. K. Park,[35] W. J. Park,[35] S. F. Pate,[53] L. Patel,[23] H. Pei,[30] J.-C. Peng,[27] H. Pereira,[17] V. Peresedov,[32] D.Yu. Peressounko,[36] R. Petti,[8,66] C. Pinkenburg,[8] R. P. Pisani,[8] M. Proissl,[66] M. L. Purschke,[8] A. K. Purwar,[41] H. Qu,[1,23] J. Rak,[33,52] A. Rakotozafindrabe,[38] I. Ravinovich,[73] K. F. Read,[55,68] S. Rembeczki,[21] K. Reygers,[47] D. Reynolds,[65] V. Riabov,[58] Y. Riabov,[58,62] E. Richardson,[44] N. Riveli,[54] D. Roach,[71] G. Roche,[42,*] S. D. Rolnick,[9] M. Rosati,[30] S. S. E. Rosendahl,[43] P. Rosnet,[42] P. Rukoyatkin,[32] P. Ružička,[29] V. L. Rykov,[59] B. Sahlmueller,[47,66] N. Saito,[34,37,59,60] T. Sakaguchi,[8] S. Sakai,[70] K. Sakashita,[59,69] V. Samsonov,[51,58] M. Sano,[70] M. Sarsour,[23] T. Sato,[70] S. Sawada,[34] K. Sedgwick,[9] J. Seele,[14] R. Seidl,[27,59,60] A.Yu. Semenov,[30] V. Semenov,[26,28] A. Sen,[23] R. Seto,[9] D. Sharma,[73] I. Shein,[26] T.-A. Shibata,[59,69] K. Shigaki,[25] M. Shimomura,[70] K. Shoji,[37,59] P. Shukla,[5] A. Sickles,[8] C. L. Silva,[30,63] D. Silvermyr,[55] C. Silvestre,[17] K. S. Sim,[35] B. K. Singh,[4] C. P. Singh,[4] V. Singh,[4] M. Slunečka,[10] A. Soldatov,[26] R. A. Soltz,[40] W. E. Sondheim,[41] S. P. Sorensen,[68] M. Soumya,[65] I. V. Sourikova,[8] F. Staley,[17] P. W. Stankus,[55] E. Stenlund,[43] M. Stepanov,[45,53] A. Ster,[74] S. P. Stoll,[8] T. Sugitate,[25] C. Suire,[56] A. Sukhanov,[8] J. Sun,[66] J. Sziklai,[74] E. M. Takagui,[63] A. Takahara,[13] A. Taketani,[59,60] R. Tanabe,[70] Y. Tanaka,[50] S. Taneja,[66] K. Tanida,[59,60,64] M. J. Tannenbaum,[8] S. Tarafdar,[4] A. Taranenko,[51,65] P. Tarján,[18] E. Tennant,[53] H. Themann,[66] T. L. Thomas,[52] T. Todoroki,[59,70] M. Togawa,[37,59] A. Toia,[66] L. Tomášek,[29] M. Tomášek,[16,29] Y. Tomita,[70] H. Torii,[25,59] R. S. Towell,[1] V-N. Tram,[38] I. Tserruya,[73] Y. Tsuchimoto,[13,25] T. Tsuji,[13] C. Vale,[8,30] H. Valle,[71]

H. W. van Hecke,[41] M. Vargyas,[19] E. Vazquez-Zambrano,[15] A. Veicht,[15,27] J. Velkovska,[71] R. Vértesi,[18,74] A. A. Vinogradov,[36] M. Virius,[16] A. Vossen,[27] V. Vrba,[16,29] E. Vznuzdaev,[58] X. R. Wang,[53] D. Watanabe,[25] K. Watanabe,[70] Y. Watanabe,[59,60] Y. S. Watanabe,[13] F. Wei,[30] R. Wei,[65] J. Wessels,[47] S. Whitaker,[30] S. N. White,[8] D. Winter,[15] S. Wolin,[27] C. L. Woody,[8] M. Wysocki,[14] W. Xie,[60] Y. L. Yamaguchi,[13,59,72] K. Yamaura,[25] R. Yang,[27] A. Yanovich,[26] J. Ying,[23] S. Yokkaichi,[59,60] Z. You,[41] G. R. Young,[55] I. Younus,[39,52] I. E. Yushmanov,[36] W. A. Zajc,[15] O. Zaudtke,[47] A. Zelenski,[7] C. Zhang,[55] S. Zhou,[12] and L. Zolin[32]
(PHENIX Collaboration)

[1]*Abilene Christian University, Abilene, Texas 79699, USA*
[2]*Institute of Physics, Academia Sinica, Taipei 11529, Taiwan*
[3]*Department of Physics, Augustana College, Sioux Falls, South Dakota 57197, USA*
[4]*Department of Physics, Banaras Hindu University, Varanasi 221005, India*
[5]*Bhabha Atomic Research Centre, Bombay 400 085, India*
[6]*Baruch College, City University of New York, New York, New York 10010, USA*
[7]*Collider-Accelerator Department, Brookhaven National Laboratory, Upton, New York 11973-5000, USA*
[8]*Physics Department, Brookhaven National Laboratory, Upton, New York 11973-5000, USA*
[9]*University of California-Riverside, Riverside, California 92521, USA*
[10]*Charles University, Ovocný trh 5, Praha 1, 116 36 Prague, Czech Republic*
[11]*Chonbuk National University, Jeonju 561-756, Korea*
[12]*Science and Technology on Nuclear Data Laboratory, China Institute of Atomic Energy, Beijing 102413, People's Republic of China*
[13]*Center for Nuclear Study, Graduate School of Science, University of Tokyo, 7-3-1 Hongo, Bunkyo, Tokyo 113-0033, Japan*
[14]*University of Colorado, Boulder, Colorado 80309, USA*
[15]*Columbia University, New York, New York 10027, USA and Nevis Laboratories, Irvington, New York 10533, USA*
[16]*Czech Technical University, Zikova 4, 166 36 Prague 6, Czech Republic*
[17]*Dapnia, CEA Saclay, F-91191 Gif-sur-Yvette, France*
[18]*Debrecen University, Egyetem tér 1, H-4010 Debrecen, Hungary*
[19]*ELTE, Eötvös Loránd University, Pázmány P. s. 1/A, H-1117 Budapest, Hungary*
[20]*Ewha Womans University, Seoul 120-750, Korea*
[21]*Florida Institute of Technology, Melbourne, Florida 32901, USA*
[22]*Florida State University, Tallahassee, Florida 32306, USA*
[23]*Georgia State University, Atlanta, Georgia 30303, USA*
[24]*Hanyang University, Seoul 133-792, Korea*
[25]*Hiroshima University, Kagamiyama, Higashi-Hiroshima 739-8526, Japan*
[26]*IHEP Protvino, State Research Center of Russian Federation, Institute for High Energy Physics, Protvino 142281, Russia*
[27]*University of Illinois at Urbana-Champaign, Urbana, Illinois 61801, USA*
[28]*Institute for Nuclear Research of the Russian Academy of Sciences, prospekt 60-letiya Oktyabrya 7a, Moscow 117312, Russia*
[29]*Institute of Physics, Academy of Sciences of the Czech Republic, Na Slovance 2, 182 21 Prague 8, Czech Republic*
[30]*Iowa State University, Ames, Iowa 50011, USA*
[31]*Advanced Science Research Center, Japan Atomic Energy Agency, 2-4 Shirakata Shirane, Tokai-mura, Naka-gun, Ibaraki-ken 319-1195, Japan*
[32]*Joint Institute for Nuclear Research, 141980 Dubna, Moscow Region, Russia*
[33]*Helsinki Institute of Physics and University of Jyväskylä, P.O. Box 35, FI-40014 Jyväskylä, Finland*
[34]*KEK, High Energy Accelerator Research Organization, Tsukuba, Ibaraki 305-0801, Japan*
[35]*Korea University, Seoul 136-701, Korea*
[36]*Russian Research Center "Kurchatov Institute," Moscow 123098, Russia*
[37]*Kyoto University, Kyoto 606-8502, Japan*
[38]*Laboratoire Leprince-Ringuet, Ecole Polytechnique, CNRS-IN2P3, Route de Saclay, F-91128 Palaiseau, France*
[39]*Physics Department, Lahore University of Management Sciences, Lahore 54792, Pakistan*
[40]*Lawrence Livermore National Laboratory, Livermore, California 94550, USA*
[41]*Los Alamos National Laboratory, Los Alamos, New Mexico 87545, USA*
[42]*LPC, Université Blaise Pascal, CNRS-IN2P3, Clermont-Fd, 63177 Aubiere Cedex, France*
[43]*Department of Physics, Lund University, Box 118, SE-221 00 Lund, Sweden*
[44]*University of Maryland, College Park, Maryland 20742, USA*
[45]*Department of Physics, University of Massachusetts, Amherst, Massachusetts 01003-9337, USA*
[46]*Department of Physics, University of Michigan, Ann Arbor, Michigan 48109-1040, USA*
[47]*Institut fur Kernphysik, University of Muenster, D-48149 Muenster, Germany*
[48]*Muhlenberg College, Allentown, Pennsylvania 18104-5586, USA*
[49]*Myongji University, Yongin, Kyonggido 449-728, Korea*
[50]*Nagasaki Institute of Applied Science, Nagasaki-shi, Nagasaki 851-0193, Japan*

[51]*National Research Nuclear University, MEPhI, Moscow Engineering Physics Institute, Moscow 115409, Russia*
[52]*University of New Mexico, Albuquerque, New Mexico 87131, USA*
[53]*New Mexico State University, Las Cruces, New Mexico 88003, USA*
[54]*Department of Physics and Astronomy, Ohio University, Athens, Ohio 45701, USA*
[55]*Oak Ridge National Laboratory, Oak Ridge, Tennessee 37831, USA*
[56]*IPN-Orsay, Universite Paris Sud, CNRS-IN2P3, BP1, F-91406 Orsay, France*
[57]*Peking University, Beijing 100871, People's Republic of China*
[58]*PNPI, Petersburg Nuclear Physics Institute, Gatchina, Leningrad region 188300, Russia*
[59]*RIKEN Nishina Center for Accelerator-Based Science, Wako, Saitama 351-0198, Japan*
[60]*RIKEN BNL Research Center, Brookhaven National Laboratory, Upton, New York 11973-5000, USA*
[61]*Physics Department, Rikkyo University, 3-34-1 Nishi-Ikebukuro, Toshima, Tokyo 171-8501, Japan*
[62]*Saint Petersburg State Polytechnic University, St. Petersburg 195251, Russia*
[63]*Universidade de São Paulo, Instituto de Física, Caixa Postal 66318, São Paulo CEP05315-970, Brazil*
[64]*Department of Physics and Astronomy, Seoul National University, Seoul 151-742, Korea*
[65]*Chemistry Department, Stony Brook University, SUNY, Stony Brook, New York 11794-3400, USA*
[66]*Department of Physics and Astronomy, Stony Brook University, SUNY, Stony Brook, New York 11794-3800, USA*
[67]*SUBATECH (Ecole des Mines de Nantes, CNRS-IN2P3, Université de Nantes) BP 20722, 44307 Nantes, France*
[68]*University of Tennessee, Knoxville, Tennessee 37996, USA*
[69]*Department of Physics, Tokyo Institute of Technology, Oh-okayama, Meguro, Tokyo 152-8551, Japan*
[70]*Institute of Physics, University of Tsukuba, Tsukuba, Ibaraki 305, Japan*
[71]*Vanderbilt University, Nashville, Tennessee 37235, USA*
[72]*Waseda University, Advanced Research Institute for Science and Engineering, 17 Kikui-cho, Shinjuku-ku, Tokyo 162-0044, Japan*
[73]*Weizmann Institute, Rehovot 76100, Israel*
[74]*Institute for Particle and Nuclear Physics, Wigner Research Centre for Physics, Hungarian Academy of Sciences (Wigner RCP, RMKI), PO Box 49, H-1525 Budapest 114, Hungary*
[75]*Yonsei University, IPAP, Seoul 120-749, Korea*
[76]*University of Zagreb, Faculty of Science, Department of Physics, Bijenička 32, HR-10002 Zagreb, Croatia*
(Received 17 May 2014; published 24 February 2015)

Measurements of bottomonium production in heavy-ion and $p+p$ collisions at the Relativistic Heavy Ion Collider (RHIC) are presented. The inclusive yield of the three Υ states, $\Upsilon(1S+2S+3S)$, was measured in the PHENIX experiment via electron-positron decay pairs at midrapidity for Au + Au and $p+p$ collisions at $\sqrt{s_{NN}} = 200$ GeV. The $\Upsilon(1S+2S+3S) \to e^+e^-$ differential cross section at midrapidity was found to be $B_{ee}d\sigma/dy = 108 \pm 38$ (stat) ± 15 (syst) ± 11 (luminosity) pb in $p+p$ collisions. The nuclear modification factor in the 30% most central Au + Au collisions indicates a suppression of the total Υ state yield relative to the extrapolation from $p+p$ collision data. The suppression is consistent with measurements made by STAR at RHIC and at higher energies by the CMS experiment at the Large Hadron Collider.

DOI: 10.1103/PhysRevC.91.024913 PACS number(s): 25.75.Dw

I. INTRODUCTION

One of the main physics programs in relativistic heavy-ion collisions is the study of heavy quarkonia yields, namely charm quark pairs (charmonia) and bottom quark pairs (bottomonia). At zero temperature, the binding energy between the heavy quark and antiquark ($Q\bar{Q}$) in these vector mesons may be described by an effective potential consisting of a confining term at large distance and Coulomb-like term at short distance [1].

When the temperature of the medium formed after the collision is higher than a transition temperature $T_c \approx 170$ MeV, the effective potential between light quark and antiquark weakens and deconfines the constituent quarks of mesons and baryons. The quark-gluon plasma (QGP) formed can be described as a dense, strongly coupled state of matter which reaches thermalization in less than 1 fm/c [2].

In the QGP medium, the effective color electric potential between Q and $\bar{Q}$ can be screened by the dense surrounding color charges. This color screening is similar to the Debye screening observed in electromagnetic plasmas [3]. The temperature at which the heavy quark state becomes unbound owing to this screening depends on the corresponding binding energy of the state. Because of the large variation in radii between the different heavy quarkonia, they are expected to become unbound at different temperatures.

There are many theoretical calculations which predict the temperature at which each quarkonium state is suppressed by color screening. A compilation of results can be found in Ref. [4], including lattice quantum chromodynamics (QCD) [5–15], QCD sum rules [4,16–20], anti-de-Sitter space/QCD [21–24], resummed perturbation theory [25,26], effective field theories [27,28], and potential models [15,29–35].

*Deceased
†PHENIX cospokesperson: morrison@bnl.gov
‡PHENIX cospokesperson: jamie.nagle@colorado.edu

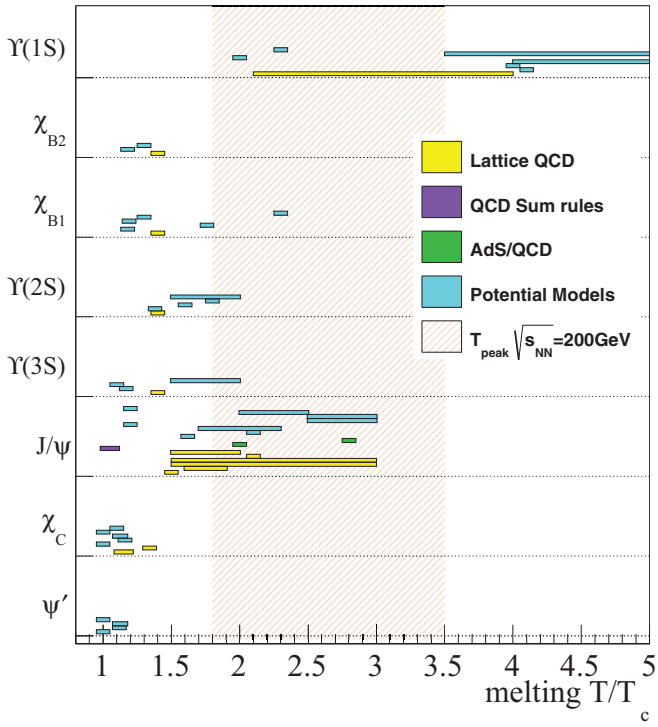

FIG. 1. (Color online) Compilation of medium temperatures relative to the critical temperature (T_c), where quarkonium states are dissociated in the QGP. Note that these estimations were performed assuming different T_c values. Each horizontal bar corresponds to one estimation and its temperature extension (when applied) represents the range where the quarkonia state undergoes a mass/size modification until it completely melts. Techniques used in calculations: lattice QCD [5–15], QCD sum rules [4,16–20], AdS/QCD [21–24], effective field theories [27,28], and potential models [15,29–35]. The shaded band from $1.8T/T_c$ to $3.5T/T_c$ represents the hydrodynamic estimation for the peak temperature reached in Au + Au collisions at 200 GeV [36].

Figure 1 shows the dissociation temperature range for several quarkonium states as expected from these models. Besides the different techniques used in these calculations, the melting range also depends on the choice of the transition temperature, the use of the internal energy or the free energy of the system for the temperature dependence of the heavy quark potential, and the criteria adopted for defining the dissociation point. No cold nuclear-matter effects have been considered in these estimations.

A comparison between hydrodynamical model calculations and the PHENIX thermal photon data [36] suggests that the peak temperature of the medium formed at RHIC in central Au + Au collisions at $\sqrt{s_{NN}} = 200$ GeV lies in the region between 300 and 600 MeV, or $1.8T_c$ and $3.5T_c$. The majority of the estimates shown in Fig. 1 indicates that only the ground states, the J/ψ and Υ(1S), remain bound at these temperatures.

PHENIX reported a strong suppression of the J/ψ yield in central Au + Au collisions compared to binary collision scaling from $p + p$ yields [37,38]. According to measurements performed in $p + p$ collisions at RHIC, $(42 \pm 9)\%$ of the J/ψ yield comes from χ_c and ψ' decays [39]. The complete suppression of these states in Au + Au collisions can explain only part of the suppression seen for the J/ψ. There are other possible contributions to J/ψ suppression and therefore the interpretation of the data is not straightforward. Other mechanisms of suppression include initial- and final-state cold nuclear-matter effects, studied in d + Au collisions by PHENIX [40,41]. There are also effects that can reduce the suppression. The dissociated charm (and anticharm) quark can undergo multiple scatterings and recombine with its former partner once the medium cools down. In addition, the presence of about 6–20 open charm pairs in each central Au + Au collision at RHIC[1] provides a good chance that the ground-state charmonium was formed by coalescence of uncorrelated charm and anticharm quarks present in the medium [43]. Thus, even if all the initially produced J/ψ's are dissociated in the QGP medium, J/ψ's can be re-created at a later stage by the coalescence process.

TABLE I. Composition of the Υ family in the dilepton channel as measured by E866/NuSea [46], CDF [47], LHCb [48], and CMS [49]. Fractions are in % and only statistical uncertainties are shown.

Exp.	System	$\Upsilon(1S)$ 9.46 $\frac{\text{GeV}}{c^2}$	$\Upsilon(2S)$ 10.02 $\frac{\text{GeV}}{c^2}$	$\Upsilon(3S)$ 10.36 $\frac{\text{GeV}}{c^2}$
E866	$p + p\sqrt{s} = 39$ GeV	69.1 ± 1.0	22.2 ± 0.9	8.8 ± 0.6
CDF	$p + \bar{p}\sqrt{s} = 1.8$ TeV	72.6 ± 2.8	17.6 ± 1.7	9.7 ± 1.4
LHCb	$p + p\sqrt{s} = 7$ TeV	73.0 ± 0.3	17.9 ± 0.2	9.0 ± 0.2
CMS	$p + p\sqrt{s} = 7$ TeV	71.6 ± 1.3	18.5 ± 0.8	10.0 ± 1.3

The probability for creating a bottomonium state through coalescence is quite small at $\sqrt{s_{NN}} = 200$ GeV, given that only about 0.07 $b\bar{b}$ pairs per central event are produced.[2] Therefore, bottomonium states are a better probe of color screening in Au + Au collisions at RHIC. Figure 1 shows that no lattice QCD or potential model calculation predicts that $\Upsilon(1S)$ will melt at a temperature lower than around $2T_c$. This is an outcome of the tighter binding energy and smaller radius of the $1S$ state compared to other quarkonium states. Some calculations suggest that the ground-state charmonium is dissociated at a temperature close to T_c [20,31,34].

Bottomonia have been measured mostly in the dilepton channel with a branching ratio around 2.5% [45]. Table I lists the fraction of the three Υ states present in the dilepton spectrum as measured at Fermilab and the Large Hadron Collider (LHC) by E866/NuSea [46], CDF [47], LHCb [48], and CMS [49]. No significant variations on the relative yields have been observed in spite of the broad collision energy range of these experiments or whether the antiproton was one of the collision particles or not. The ground-state $\Upsilon(1S)$ has many feed-down contributions from excited states. The CDF experiment reported the fraction of these contributions [50], which can be seen in Table II.

[1]This estimation is based on the $c - \bar{c}$ total cross section reported in Ref. [42] and 1000 binary collisions in very central Au + Au events.

[2]Estimation based on the total $b\bar{b}$ cross section published in Ref. [44].

TABLE II. Feed-down fractions of the $\Upsilon(1S)$ state in $p+p$ collisions as measured by CDF for $p_T > 8$ GeV/c [50].

Source	Fraction $\pm$ stat $\pm$ syst
Direct $\Upsilon(1S)$	$0.509 \pm 0.082 \pm 0.090$
$\Upsilon(2S)$	$0.107 \pm 0.077 \pm 0.048$
$\Upsilon(3S)$	$0.008 \pm 0.006 \pm 0.004$
χ_{B1}	$0.271 \pm 0.069 \pm 0.044$
χ_{B2}	$0.105 \pm 0.044 \pm 0.014$

Fermilab experiments found no modification of the relative yields in cold nuclear matter as measured in $p+d$ [46] and $p+A$ [51]. The initial-state effects on bottomonia production were investigated by E605 [52], E772 [51], and E866/NuSea [46] in $p+A$ collisions at $\sqrt{s_{NN}} = 38.8$ GeV with targets of ^{2}H, C, Ca, and Fe. The Υ yields are suppressed by ~5% for incident gluon momentum fraction $x_2 \sim 0.1$. The suppression gets stronger for larger x_2, reaching a level of ~15% at $x_2 \sim 0.3$. PHENIX measured the medium modification of the Υ family $(1S+2S+3S)$ yield in $d+$Au collisions at $\sqrt{s_{NN}} = 200$ GeV [53]. The result is consistent with no modification within the large statistical uncertainties at $x_2 \sim 10^{-2}$ and presents a one-standard-deviation suppression at $x_2 \sim 0.2$, which is consistent with the Fermilab results and the STAR experiment at midrapidity in $d+$Au collisions [54]. The RHIC results can be accounted for by a combination of initial-state effects, calculated by the parton modification function EPS09 [11], and quarkonium breakup when crossing the cold nuclear matter.

QGP effects on Υ production were studied at the LHC by the CMS experiment [55] using Pb + Pb collisions at $\sqrt{s_{NN}} =$ 2.76 TeV. The excited state $\Upsilon(2S)$ is more suppressed than the $\Upsilon(1S)$ and the $\Upsilon(3S)$ state is not seen in CMS data. This is qualitatively consistent with expectations of the effects of color screening from several models discussed earlier. The question which arises is whether or not the suppression also happens at lower energies and in an environment with a much smaller number of bottom quarks present in the medium.

This paper reports the measurement of the inclusive $\Upsilon(1S+2S+3S)$ yield at $|y| < 0.35$ in Au + Au collisions at $\sqrt{s} = 200$ GeV. Section II describes the experimental apparatus and the data sample used in the measurement. Section III details the signal extraction, detector response, and systematic uncertainties involved in this measurement. The results and comparisons with other measurements and models are presented in Sec. IV. The final conclusions are presented in Sec. V.

II. EXPERIMENTAL APPARATUS AND DATA SET

The PHENIX experiment measures quarkonia at midrapidity through their dielectron decays with the two-arm central spectrometers [56] shown in Fig. 2. The central-arm detectors measure electrons, photons, and hadrons over pseudorapidity of $|\eta| < 0.35$ with each arm covering azimuthal angle $\Delta\phi = \pi/2$. Charged-particle tracks in the central arms are reconstructed using the drift chambers (DCs), the pad chambers, and the collision point. Electron candidates are selected using

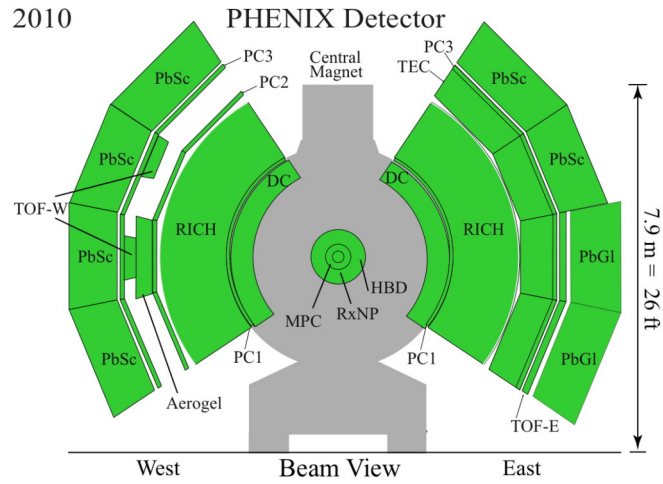

FIG. 2. (Color online) The PHENIX Central Arm Spectrometers for the 2010 data-taking period.

information from the ring-imaging Čerenkov detector (RICH) and the electromagnetic calorimeter (EMCal) [39]. The total radiation length before the DC during the 2006 $p+p$ run was 0.4%. During the 2010 Au + Au run more material was introduced from the hadron blind detector (HBD), which added 2.4% radiation lengths to what the detector had in 2006. In the 2010 run, the magnetic field configuration was also modified to cancel the field in the HBD volume, decreasing the momentum resolution by about 25%.

Beam interactions were selected with a minimum bias (MB) trigger that requires at least one hit (two in Au + Au collisions) per beam crossing in each of the two beam-beam counters (BBCs) placed at $3.0 < |\eta| < 3.9$. In the Au + Au data set, this was the only trigger used. A dedicated EMCal-RICH trigger (ERT) was used in coincidence with the MB trigger during the 2006 $p+p$ data acquisition. The ERT required a minimum energy in any 2×2 group of EMCal towers, corresponding to $\Delta\eta \times \Delta\phi \approx 0.02 \times 0.02$ rad, plus associated hits in the RICH. The minimum EMCal energy requirement was 400 MeV for the first half of the run and 600 MeV for the second half.

The collision point along the beam direction was determined with a resolution of 1.5 cm in $p+p$ collisions and 0.5 cm in Au + Au collisions by using the difference between the time signals measured between the two BBC detectors. The collision point was required to be within ± 30 cm of the nominal center of the detector in $p+p$ collisions and ± 20 cm in Au + Au collisions. The 2006 data sample was taken from $N_{pp} = 143 \times 10^9$ MB events, corresponding to an integrated luminosity of 6.2 pb^{-1}. The 2010 data sample was obtained from $N_{\mathrm{AuAu}} = 5.41 \times 10^9$ MB events, corresponding to 0.9 nb^{-1}.

In $p+p$ collisions, electron candidates were identified by requiring at least one fired phototube within an annulus $3.4 < R_{\mathrm{ring}}$ [cm] < 8.4 centered in the projected track position on the RICH. The RICH is filled with a CO_2 radiator at 1 atm. Pions with momentum larger than 4.8 GeV/c can also produce Čerenkov light in the RICH. Electron candidates are also required to be associated with an energy cluster in the

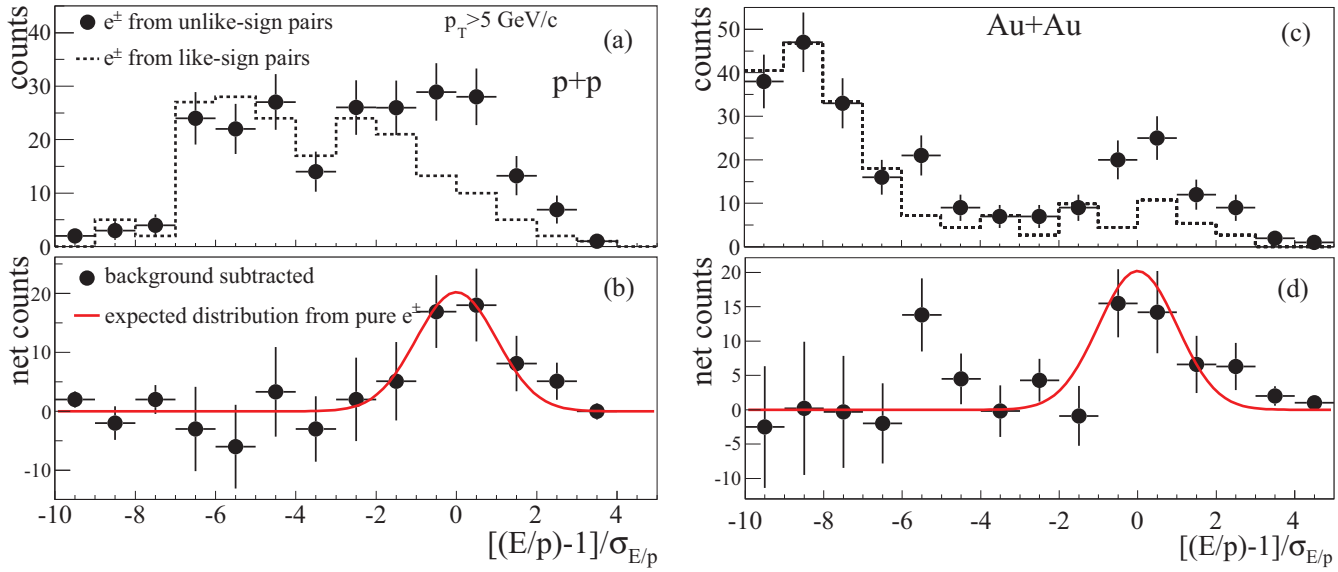

FIG. 3. (Color online) Distribution of the parameter used to identify electrons with the EMCal. E/p is the ratio between the energy deposited by the particle in the EMCal cluster and its momentum, $\sigma_{E/p}$ is the variance of the expected energy/momentum expected for electrons. The sample shown in (a) from $p+p$ collisions and (c) from Au + Au collisions is from unlike-sign electron pairs (containing signal + combinatorial background) and like-sign pairs (containing only background). Panels (b) and (d) are the background-subtracted distributions along with the expected line shape from pure electrons.

EMCal that falls within the $4\sigma_{\text{position}}$ of the projected track position and within $4\sigma_{E/p}$ of the expected energy/momentum ratio for electrons, where σ represents one standard deviation in the position and energy + momentum resolution of the EMCal + DC determined using electrons from fully reconstructed Dalitz decays. Figure 3 shows the distribution of the parameter used to select electrons in the EMCal using electron candidates used in high-mass dielectrons with $p_T > 5$ GeV/c, above the Čerenkov threshold. Hadron contamination appears as an enhancement of this distribution for negative values. The distribution, after subtracting the background mainly composed of hadrons, represents a clean sample of electrons for $(E/p) - 1 < 4\sigma_{E/p}$.

In the Au + Au analysis, the cuts were optimized by looking at the parameters in the detector simulations using generated $\Upsilon \to e^+e^-$ decays embedded into real data for the signal and the real data like-sign dielectrons as a background. As a result of the optimization, we require the following:

(i) at least two fired phototubes within an annulus $3.4 < R_{\text{ring}}$ [cm] < 8.4 centered in the projected track position on the RICH;
(ii) $\chi^2/npe0 < 25$, a variable defined as χ^2-like shape of the RICH ring associated with the track over the number of photoelectrons detected in the ring;
(iii) the displacement between the ring centroid and the track projection should be smaller than 7 cm;
(iv) EMCal cluster-track matching should be smaller than $3\sigma_{\text{position}}$;
(v) EMCal cluster energy/momentum ratio should be larger than $-2.5\sigma_{E/p}$.

These tighter cuts allowed a better hadron rejection, as can be seen in Fig. 3(c) compared to the $p+p$ sample in Fig. 3(a).

Figure 4 shows the reconstructed invariant mass distribution for the three Υ states from PHENIX detector simulations in the 2006 $p+p$ run configuration and in 2010 Au + Au configuration. The detector is not able to separate the three

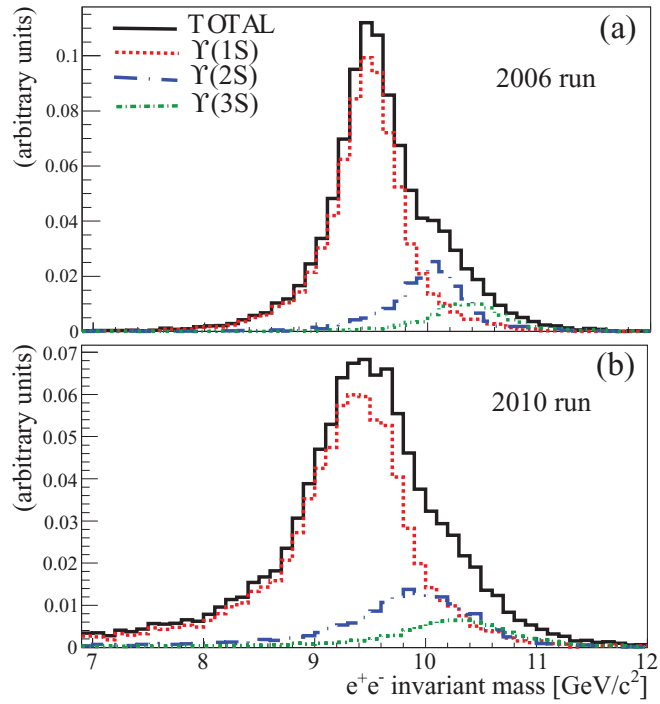

FIG. 4. (Color online) Invariant mass distribution of simulated $\Upsilon(1S+2S+3S)$ using the PHENIX detector simulation and relative Υ yields from CDF experiment [47] in the 2006 run (a) and the 2010 run (b) detector configurations.

states and a single peak should be observed. In the 2010 detector configuration the addition of more material in the detector introduced more bremsstrahlung for the electrons increasing the low-mass tail of the peaks.

III. ANALYSIS PROCEDURE

A. Dielectrons from Υ in the central arms

The invariant mass was calculated for all electron pairs. Dielectron contributions to Υ decays are clearly identified as a peak in the unlike-sign invariant mass distributions around the Υ mass range $8.5 < M_{ee}$ [GeV/c^2] < 11.5 (Fig. 5). There were 12 unlike- and one like-sign dielectron within this mass region from the $p+p$ sample. In the Au + Au sample there were 22 unlike- and 3 like-sign pairs in the same mass region.

Figure 6 shows the $p+p$ dielectron mass spectrum over an extended mass region after the like-sign distribution (used to estimate combinatorial background) has been subtracted from the unlike-sign data. Figure 7 shows the same invariant mass spectrum in the Υ mass region for $p+p$ and Au + Au data. The line shape of the Υ mass peak determined from simulations (Fig. 4) cannot be validated by the real data given the low statistics in both $p+p$ and Au + Au samples. In addition, the relative contributions from different Υ states are unknown in Au + Au data. The number of Υ counts was determined from a direct count of unlike-sign and like-sign dielectrons in the Υ mass region and the fraction of correlated

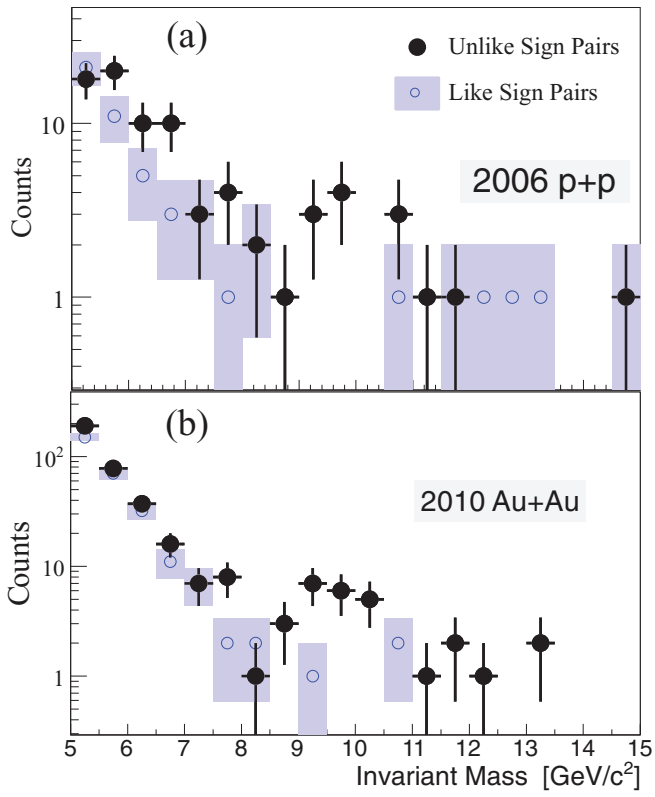

FIG. 5. (Color online) Invariant mass distribution of unlike-sign and like-sign dielectrons in the Υ mass region taken from $p+p$ (a), and Au + Au collisions (b).

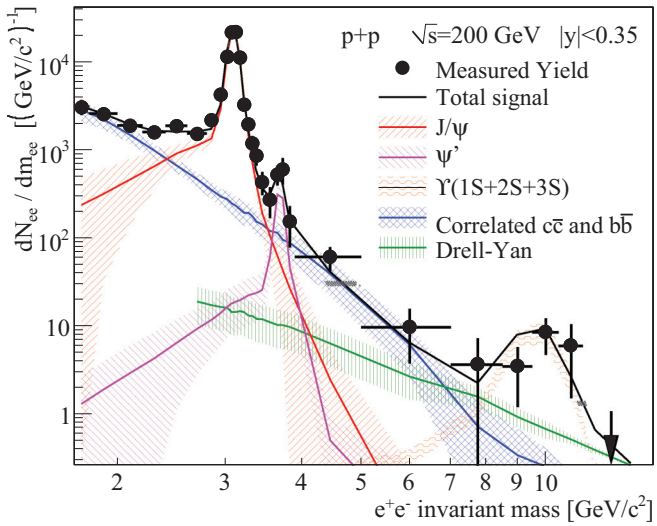

FIG. 6. (Color online) Fitted components to the correlated dielectron mass spectrum in the $p+p$ sample. The bands correspond to the uncertainties obtained from the fit, changes in the heavy flavor generator, and theoretical uncertainties in the Drell-Yan contribution.

background $f_{\rm cont}$ in the same mass range. Given the low counts for the signal and background, Poisson statistics precludes the use of a simple subtraction. Therefore, the Υ signal is determined from

$$N_\Upsilon = \langle s \rangle_P (1 - f_{\rm cont}), \tag{1}$$

where $\langle s \rangle_P$ is the average signal from a joint Poisson distribution from the foreground unlike-sign f and background like-sign b dielectron counts in the Υ mass region [39],

$$P(s) = \sum_{k=0}^{f} \frac{(b+f-k)!}{b!(f-k)!} \frac{1}{2} \left(\frac{1}{2}\right)^{b+f-k} \frac{s^k e^{-s}}{k!}, \tag{2}$$

and the statistical uncertainty corresponds to one standard deviation of the $P(s)$ distribution.

B. Estimation of the continuum contribution

The correlated background underneath the Υ region is determined from fits of the expected mass dependence of Drell-Yan, correlated electrons from B meson decays, and possible contamination of hadrons within jets.

The Drell-Yan contribution was estimated from next-to-leading order (NLO) QCD calculations [57]. These calculations are known to reproduce lower- and higher-energy data at Fermilab [58,59]. The calculated cross section was used to generate dielectrons propagated through the GEANT [60] based detector simulation. The Drell-Yan contribution is modified by isospin and initial-state effects in Au + Au collisions. After calculating the Drell-Yan cross section for $p+n$ and $n+n$ collisions, we found that the Au + Au cross section per binary collision is $f_{\rm iso} = 89\%$ of that of $p+p$ collisions because of the isospin effect. The initial-state effects were accounted for by using a parton modification factor from the EPS09 parametrization, $R_q^{\rm DY}(Q^2, x_1, x_2)$, for both Au nuclei. The expected Drell-Yan yield in Au + Au collisions ($Y_{\rm DY}^{\rm AuAu}$)

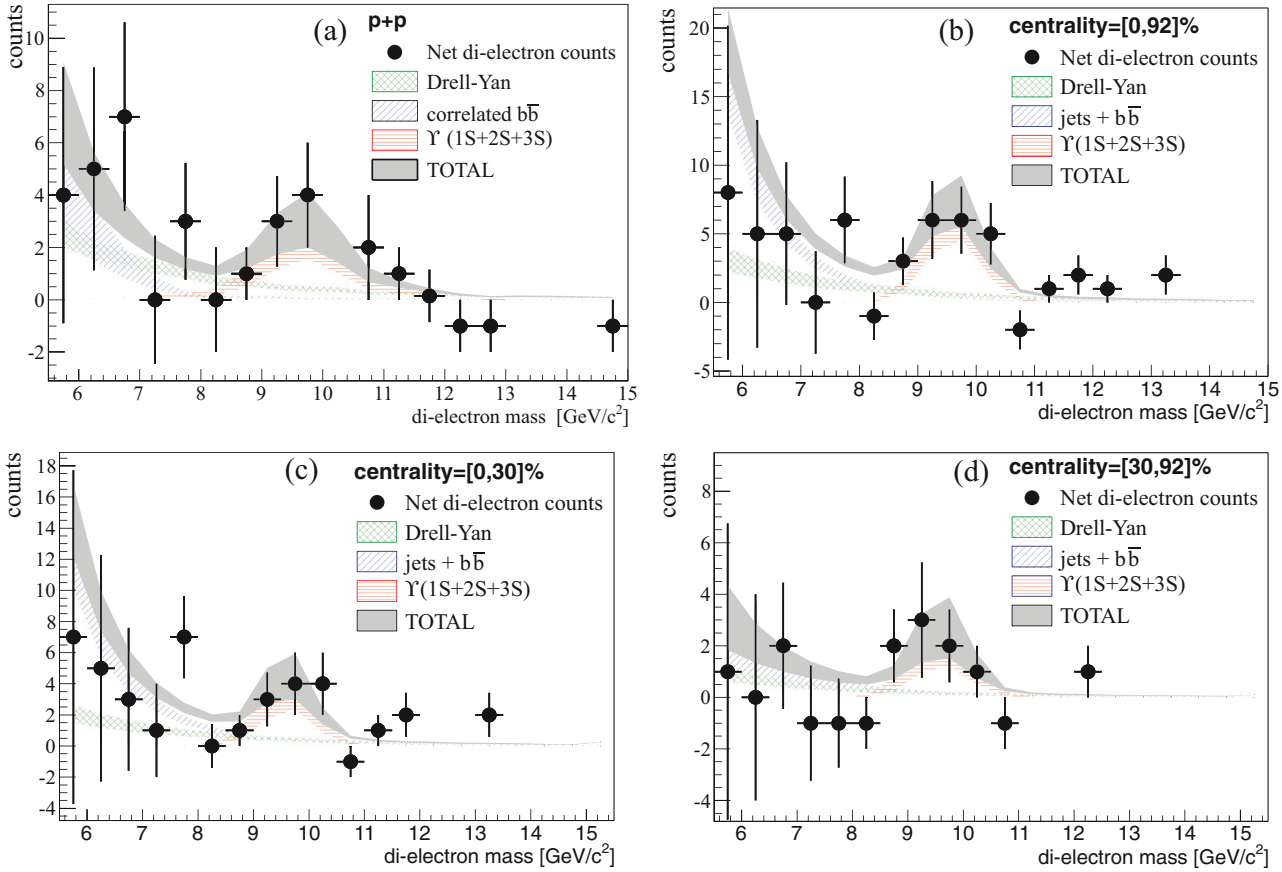

FIG. 7. (Color online) Fits to the correlated dielectron mass distribution around the ϒ region obtained in $p+p$ collisions (a) and Au + Au collisions in three centrality bins (b),(c),(d). The bands correspond to fitting and theoretical uncertainties for the Drell-Yan estimation. Fitting results are used only for correlated background estimations.

relative to the yield in $p+p$ collisions ($Y_{\rm DY}^{pp}$) is

$$\frac{Y_{\rm DY}^{\rm AuAu}(M_{ee})}{N_{\rm coll}} = Y_{\rm DY}^{pp}(M_{ee})\, f_{\rm iso} R_q^{\rm DY}(Q^2,x_1,x_2), \qquad (3)$$

where $N_{\rm coll}$ is the number of binary collisions. Q^2, x_1, and x_2 are taken event by event from a PYTHIA simulation [61]. Theoretical uncertainties from the NLO calculation, EPS09 quark modification factor [$R_q^{\rm DY}(Q^2,x_1,x_2)$] and overall detector response were accounted for in the Drell-Yan contribution.

The line shape of the correlated high-mass dielectron distribution from heavy flavor decays in $p+p$ collisions was studied in detail in Ref. [39]. Two approaches were used: (1) a dielectron generator using the measured p_T distribution of single electrons from heavy flavor with a random opening angle and (2) a heavy flavor simulation from PYTHIA in the hard scattering mode to emulate NLO contributions. Both generated dielectron distributions were introduced into the detector simulation and reconstructed like the real data. The mass distribution from heavy flavor decays was normalized according to a fit to the dielectron spectrum starting at an invariant mass at 1.7 GeV/c^2, thus including the J/ψ and the ψ' peaks. Figure 6 shows the overall dielectron fit extended to the ϒ region. The uncertainty bands represent the quadratic sum of the fit uncertainties and the differences between approaches (1) and (2). The Drell-Yan band represents the quadratic sum of theoretical uncertainties and detector response uncertainties. The extrapolation of the heavy flavor contribution to the ϒ mass range $8.5 < M_{ee}$ [GeV/c^2] < 11.5 in $p+p$ data yields 0.29 ± 0.12 counts, which corresponds to 3.9 ± 1.7 pb. The PYTHIA simulation, including parton shower terms, yields an estimate that the correlated bottom contribution in this mass range is 3.2 pb, in agreement with the fit extrapolated result.

Jets can contribute to the correlated background in two ways: Dalitz decays from π^0 pairs within the jet and correlated hadron pair contamination. For a π^0 pair to produce a correlated electron pair in the ϒ mass region, each of the π^0's should have a transverse momentum larger than the mass of the ϒ, which is a possibility ruled out by the current statistics. Figure 3 shows an insignificant hadron contamination in the high-mass dielectrons in $p+p$ data after combinatorial background subtraction. Hadron contamination was found to be negligible within uncertainties. Contributions from electron-hadron correlations are also assumed to be negligible.

The resulting continuum fraction in the selected mass range is $f_{\rm cont}^{pp} = 13 \pm 4\%$ in the $p+p$ sample. The continuum fraction was also determined with a maximum likelihood fit using the combinatorial background, Drell-Yan, B meson, and ϒ line shapes with free parameters for their scales, except

TABLE III. Summary of values used in BdN/dy (5) and R_{AA} (7) calculations.

Value	$p+p$	Au + Au 0%–92%	Au + Au 0%–30%	Au + Au 30%–92%
$N_{\rm unlike} - N_{\rm like}$	$10.5^{+3.7}_{-3.6}$	$18.3^{+5.0}_{-5.2}$	$11.2^{+3.8}_{-4.0}$	$6.4^{+3.3}_{-3.5}$
$f_{\rm cont}$	0.13 ± 0.04	0.216 ± 0.045	0.270 ± 0.063	$0.186^{+0.065}_{-0.060}$
$N_{\rm BBC} \times 10^9$	143	5.40	1.62	3.35
c	0.70	1	1	1
Acc $\times \varepsilon$	$(1.64 \pm 0.25)\%$	$(0.65 \pm 0.13)\%$	$(0.58 \pm 0.11)\%$	$(0.96 \pm 0.18)\%$
$N_{\rm coll}$	1	258 ± 25	644 ± 63	72 ± 7
$N_{\rm part}$	2	109 ± 4	242 ± 4	45 ± 2

the combinatorial background which has a fixed scale. The total continuum found in this manner was consistent with that estimated with a fixed Drell-Yan scale. The fit (without any hadron contribution) provides a good description of the mass distribution.

We cannot calculate the continuum contributions in Au + Au collisions in the same way as we do for $p+p$ collisions given the unknown nuclear modification of bottom quarks. Contributions from correlated hadrons may also start to be significant in a high-occupancy environment. We thus perform a fit to separate the continuum background from the Υ signal. The dielectron spectrum is described by the function

$$
\begin{aligned}
f(m) &= N_{\rm like} Y_{\rm like}(m) + Y_{\rm DY}(m) + N_{b\bar{b},{\rm jet}} Y_{b\bar{b},{\rm jet}}(m) + Y_{\Upsilon}(m), \\
N_{\rm like} &= \frac{2\sqrt{N_{e^+e^+} N_{e^-e^-}}}{\int Y_{\rm like}(m)\, dm}, \\
N_{b\bar{b},{\rm jet}} &= \left[N_{\rm cont} - \int_{m_{\rm low}}^{m_{\rm high}} Y_{\rm DY}(m) dm \right], \\
Y_{\Upsilon}(m) &= \frac{N_{\rm g}}{\sqrt{2\pi}\sigma_{\rm g}} \exp\left[-\frac{1}{2} \left(\frac{m - 9.5}{\sigma_{\rm g}} \right)^2 \right],
\end{aligned}
\tag{4}
$$

where $N_{\rm like} \sim 1$ is the normalization of the like-sign distribution [36], $N_{e^+e^+} + N_{e^-e^-} = 2613$ is the number of like-sign dielectron pairs over the mass range $5 < M_{ee}$ [GeV/c^2] < 15, $Y_{\rm like}(m)$ is the like-sign dielectron mass distribution from real data which account for the combinatorial background and a fraction of the correlated background, $Y_{\rm DY}(m)$ is the Drell-Yan contribution as calculated in Eq. (3), $m_{\rm low} = 8.5$ GeV/c^2 and $m_{\rm high} = 11.5$ GeV/c^2 define the mass range used in the continuum normalization, $N_{\rm cont}$ is the continuum contribution in the Υ mass region, $Y_{\Upsilon}(m)$ is a Gaussian function accounting for the Υ peak, where $\sigma_{\rm g}$ is the effective peak width of all three Υ states combined, and $Y_{b\bar{b},{\rm jet}}(m)$ is a function normalized in the Υ mass range which accounts for the correlated open bottom and hadrons from jets. We assumed both a power law and an exponential function for the correlated bottom and jet contributions

$$
Y_{b\bar{b},{\rm jet}}(m) = \begin{cases} (\alpha+1) m^{\alpha} \big/ \left(m_{\rm high}^{\alpha-1} - m_{\rm low}^{\alpha-1} \right), \\ \alpha e^{\alpha m} / \left(e^{\alpha m_{\rm high}} - e^{\alpha m_{\rm low}} \right). \end{cases}
$$

The parameters $N_{\rm cont}$, α, $N_{\rm g}$, and $\sigma_{\rm g}$ were fit to the unlike-sign dielectron spectrum between 5 and 16 GeV/c^2 using a maximum likelihood method. Figure 7 shows the $f(m) - N_{\rm like} Y_{\rm like}(m)$ fitting result assuming a power law function for the bottom-jet contribution. The bands represent the fit and theoretical uncertainties. The continuum estimate changes by up to 0.9% depending on the choice of the bottom + jet contribution function $[Y_{b\bar{b},{\rm jet}}(m)]$. Table III lists the number of net counts and the continuum fraction for $p+p$ and three centrality ranges in the Au + Au data. The fraction of continuum in Au + Au data obtained from these fits was found to be larger than in $p+p$ data. This may reflect that the nuclear modification of Drell-Yan in Au + Au is small compared to the Υ yield modification.

C. Mass cut efficiency

The Υ count is all made in the mass range $8.5 < M_{ee}$ [GeV/c^2] < 11.5. The reconstructed Υ family peaks may have some contribution at masses out of this range. According to the detector simulation using the CDF results [50] for the relative yields, the mass range $8.5 < M_{ee}$ [GeV/c^2] < 11.5 contains a fraction $\varepsilon_{\rm mass} = 0.94 \pm 0.05$ of the $\Upsilon(1S+2S+3S)$ yield in the 2006 $p+p$ data set. The uncertainty of this estimate comes from the mass fit to the $p+p$ data and from the difference between real data and simulations. In the Au + Au analysis, the evaluation of the detector occupancy effect on the efficiency included the mass cut used in the analysis. Variations in the detector mass resolution during this study indicate a systematic uncertainty in the mass cut efficiency of 6% in Au + Au data. The number of Υ counts has a 2% variation when the normalization of the like-sign dielectrons ($N_{\rm like}$) is taken from different mass ranges. This is assigned as a systematic uncertainty on the yield.

D. Detector response

The GEANT-based detector simulation was tuned as described in Ref. [39]. The acceptance and efficiency in this analysis was obtained from $\Upsilon(1S+2S+3S)$ dielectron decays generated by PYTHIA, requiring that they fall into a rapidity range of $|y| < 0.5$. The relative yield between Υ states were taken to be those reported by CDF [50]. This same detector simulation was used to estimate the detector response for the heavy flavor and Drell-Yan background line shapes, as described in the previous section.

In the $p+p$ sample, the overall acceptance and efficiency Acc $\times \varepsilon$ for Υ's calculated from simulations was found to be $(2.33 \pm 0.23)\%$ in the $|y| < 0.5$ rapidity region. The uncertainty of this estimate is from variations in the detector performance during the run, mismatches between the detector

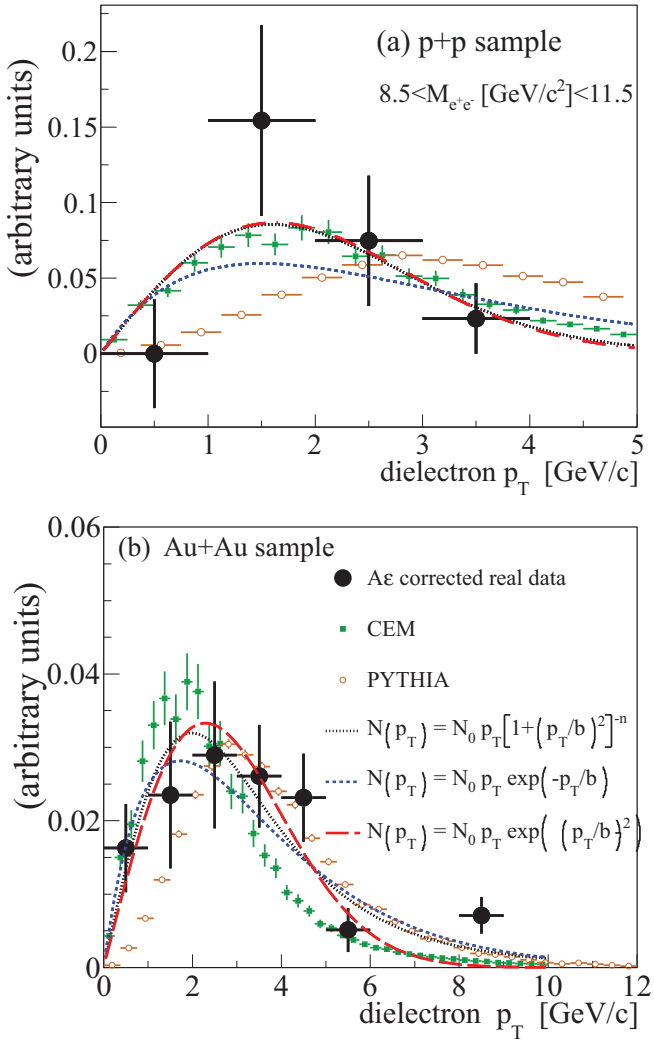

FIG. 8. (Color online) Transverse momentum dependence of acceptance corrected dielectron net counts in the Υ mass region from $p+p$ (a) and centrality integrated Au + Au (b) collisions. The lines are functions and Υ yield estimations (color evaporation model (CEM) [62] and PYTHIA [61]) fitted to the distributions.

simulation and the detector activity in real data, and variations of the p_T shape introduced in simulation [Fig. 8(a)].

The BBC trigger samples a cross section of $\sigma_{pp} \times \varepsilon_{\mathrm{BBC}} = 23 \pm 2.2$ mb in $p+p$ collisions, according to Vernier scans [63]. However, it samples a larger fraction of the cross section when the collision includes a hard scattering process. Studies with high-$p_T \pi^0$ yields showed an increase of the luminosity scanned by the BBC by a factor of $1/\varepsilon_{\mathrm{BBC}^{\mathrm{hard}}}$, $\varepsilon_{\mathrm{BBC}}^{\mathrm{hard}} = (0.79 \pm 0.02)$ [64]. In Au + Au data the BBC scans $92 \pm 3\%$ of the total Au + Au inelastic cross section and there is no bias from hard scattering ($\varepsilon_{\mathrm{BBC}}^{\mathrm{hard}} = 1$). The EMCal-RICH trigger (ERT) efficiency of dielectrons was found to be $(79.6 \pm 3.6)\%$ in the $p+p$ sample when emulating the ERT in MB data. The ERT was not used for the Au + Au data.

In the Au + Au data, the electron identification cuts were tighter, resulting in a calculated acceptance and efficiency Acc $\times \varepsilon = 1.41 \pm 0.05\%$ [point at 85% centrality in Fig. 9(b)]. To quantify additional inefficiencies from the

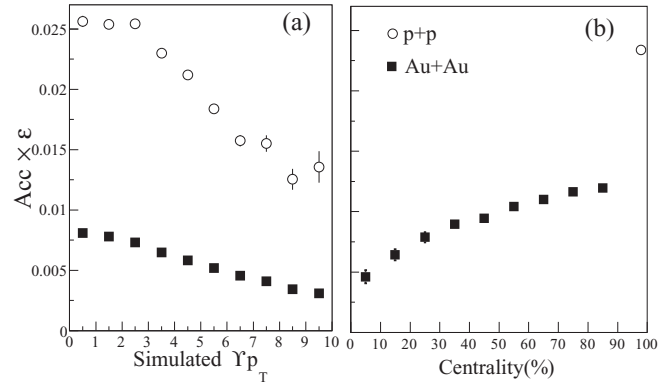

FIG. 9. Dependence of the acceptance × efficiency for detected Υ dielectron decays in $p+p$ and Au + Au collisions on (a) transverse momentum in 0%–92% centrality and (b) collision centrality. The bars represent statistical uncertainties in the simulation.

detector occupancy, the raw detector signal from simulated Υ dielectron decays was embedded in real raw data. The simulated Υ was generated at the same collision point measured in the real event. The reconstruction, fitting, and mass cuts of the embedded data were the same as those used in real data analysis. The p_T and collision centrality dependence of the resulting fraction of Υ counts in the reconstructed embedded data are shown in Fig. 9. The big difference between the detector efficiency obtained in $p+p$ data and peripheral Au + Au reflects the tight cuts needed in Au + Au because of the larger occupancy and additional material in front of the detector in the 2010 run.

Because we do not have the statistic precision to determine the transverse momentum distribution of the Υ, we must employ models for the p_T dependence to determine an overall acceptance and efficiency. Five functions were used for the p_T distribution: a shape from generated Υ decays in PYTHIA, a prediction from the color evaporation model [62], and three fitted functions $f(p_T)$ to the acceptance corrected real data distribution (Fig. 8). The p_T integrated acceptance and efficiency is determined by an average using the p_T dependence shown in Fig. 9 and these functions as weights. The difference between these calculations and the default

TABLE IV. Summary of the relative systematic uncertainties involved in BdN/dy calculations.

Systematic	Uncertainty	
	$p+p$ (%)	Au + Au (%)
Acceptance	7.5	7.0
Electron identification	1.1	5.0
Simulation input	7.8	7.9
Mass cut efficiency	6.3	5.0
Continuum contribution	5	5.8–8.6
Acceptance fluctuation	7.3	14.0
ERT efficiency	4.5	NA
Occupancy effect	NA	2.0–7.5
Combinatorial background	2.0	2.0
Total	16.1	20.7–21.2

TABLE V. Summary of the measured Υ invariant multiplicities, BdN/dy, for one $p+p$ three Au + Au data sets.

Centrality (%)	BdN/dy
$p+p$ ($\times 10^9$)	$2.7 \pm 0.9(\text{stat}) \pm 0.4(\text{syst})$
0–92 ($\times 10^7$)	$4.1^{+1.1}_{-1.2}(\text{stat}) \pm 0.9(\text{syst})$
0–30 ($\times 10^7$)	$8.7^{+2.9}_{-3.1}(\text{stat}) \pm 1.8(\text{syst})$
30–92 ($\times 10^7$)	$1.6^{+0.8}_{-0.9}(\text{stat}) \pm 0.3(\text{syst})$

weighing using PYTHIA as an input is within 7.8% in $p+p$ and 7.9% in Au + Au samples.

The final values for the efficiency in our wide centrality bins are also sensitive to the true centrality dependence of the Υ production. To estimate this systematic uncertainty we assume two different centrality dependence models: (1) binary collision scaling and (2) participant collision scaling. Within our centrality ranges, we find that these two models yield less than a 7% difference and we include this in our occupancy systematic uncertainty.

IV. RESULTS

The $\Upsilon \to e^+e^-$ invariant multiplicity at midrapidity, BdN/dy, is calculated by

$$B\frac{dN}{dy} = \frac{1}{\Delta y}\frac{N_\Upsilon}{(N_{\text{BBC}}/c)\text{Acc}\varepsilon}, \tag{5}$$

where B is the dielectron branching ratio, N_Υ is the number of Υ candidates in the data set as defined in (1), $\Delta y = 1$ corresponds to the rapidity range used in simulation (± 0.5), N_{BBC} is the number of analyzed events, $c = \varepsilon_{\text{BBC}}/\varepsilon^{\text{hard}}_{\text{BBC}}$ is a correction factor accounting for the limited BBC efficiency and the trigger bias present in events which contain a hard scattering in $p+p$ collisions as explained in Sec. III D, Acc is the Υ acceptance and ϵ is the Υ reconstruction efficiency which includes the ERT efficiency. Table III summarizes the numbers used to calculate the Υ yields using Eq. (5).

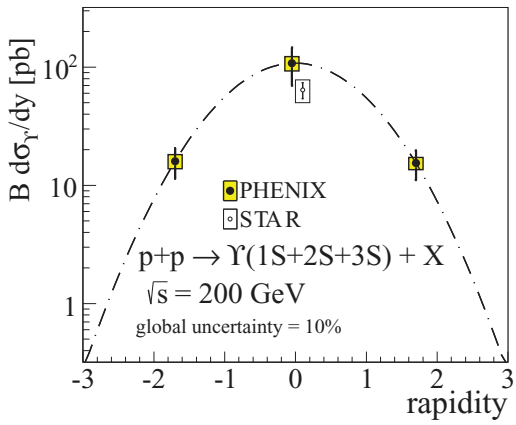

FIG. 10. (Color online) Rapidity dependence of $\Upsilon(1S+2S+3S)$ yield measured by PHENIX, forward rapidity result from [53], and STAR midrapidity from [54]. The dashed line is a Gaussian function fitted to the points. The points at zero rapidity are shifted for clarity.

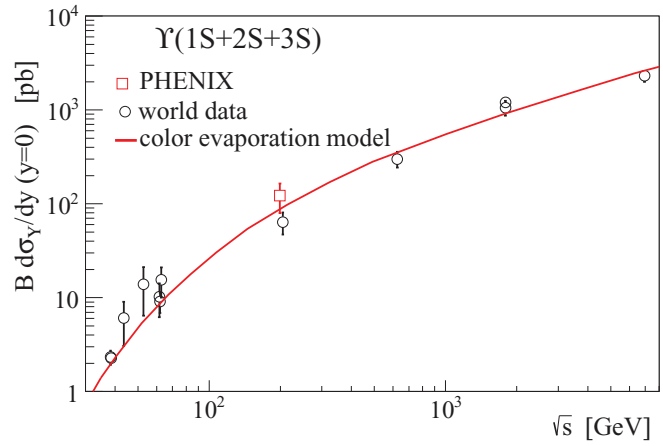

FIG. 11. (Color online) Energy dependence of the $\Upsilon(1S+2S+3S)$ differential cross section at midrapidity in $p+p$ and $p+\bar{p}$ collisions [49,52,54,65–72]. The curve is the estimation using the color evaporation model [62].

Table IV details the systematic uncertainties involved in the yield calculation. The resulting invariant multiplicities are reported in Table V.

The $\Upsilon(1S+2S+3S)$ cross section in $p+p$ collisions is

$$B\left.\frac{d\sigma_\Upsilon}{dy}\right|_{|y|<0.5} = B\frac{dN}{dy} \times \sigma_{\text{pp}} = 108 \pm 38(\text{stat}) \pm 15(\text{syst}) \pm 11(\text{lum})\ \text{pb}, \tag{6}$$

where $\sigma_{\text{pp}} = 42$ mb is the $p+p$ inelastic cross section at $\sqrt{s} = 200$ GeV.

Figure 10 shows the rapidity dependence of Υ measured in $p+p$ collisions by PHENIX in the mid- (this analysis) and forward rapidities [53] and the STAR result at midrapidity [54]. Figure 11 presents the collision energy dependence of the differential cross section at midrapidity along with a

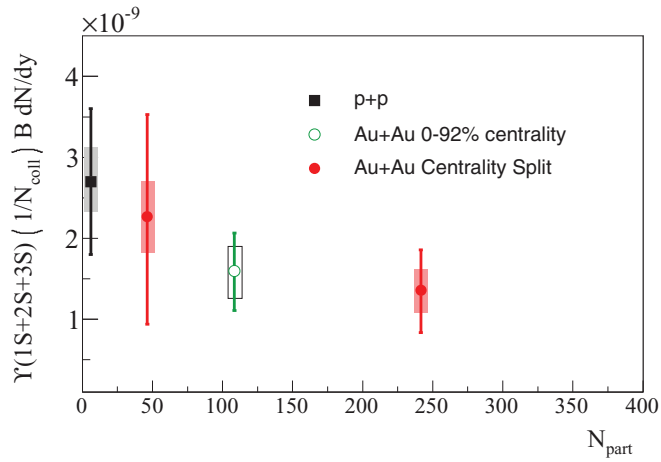

FIG. 12. (Color online) The N_{coll} normalized invariant yield of Υ's produced during the 2006 $p+p$ and the 2010 Au + Au operations, as a function of N_{part}.

TABLE VI. Summary of the measured Υ nuclear modification factors, R_{AA}, for Au + Au data sets.

Centrality (%)	R_{AA}
0–92	$0.58 \pm 0.17(\text{stat}) \pm 0.13(\text{syst}) \pm 0.23(\text{global})$
0–30	$0.50 \pm 0.18(\text{stat}) \pm 0.11(\text{syst}) \pm 0.20(\text{global})$
30–92	$0.84^{+0.45}_{-0.48}(\text{stat}) \pm 0.18(\text{syst}) \pm 0.34(\text{global})$

NLO calculation using the color evaporation model for the bottomonium hadronization [62].

In addition to the Au + Au 0%–92% centrality sample, we present data in two centrality bins, 0%–30% most central, and 30%–92% most central. Using a Monte Carlo simulation based on the Glauber model in Ref. [73], we estimated N_{coll}, the average number of binary nucleon-nucleon collisions, and N_{part}, the average number of participants, for all data samples. Figure 12 shows the N_{coll} normalized invariant yield of Υ decays as a function of the number of participants. For central Au + Au collisions, we observe a reduction of the yield relative to a pure N_{coll} xoscaling that is typical of hard scattering processes.

The nuclear modification factors for the binned and integrated 0%–92% centrality data set (R_{AA}) were calculated as

$$R_{AA} = \frac{dN/dy_{\text{AuAu}}}{\langle N_{\text{coll}} \rangle dN/dy_{\text{pp}}} \tag{7}$$

and are reported in Table VI. A global uncertainty of 40% is obtained from the quadratic sum of the relative uncertainty from 38% $p + p$ data (statistical + systematic) and 12% from the Glauber estimate of the number of collisions. We assume that none of the systematic uncertainties are correlated between $p + p$ and Au + Au samples given the different collision environment and changes in the detector configuration between the 2006 and 2010 runs, namely, active area differences and the installation of the HBD in 2010, which increased the radiation length from 0.4% to 2.8%.

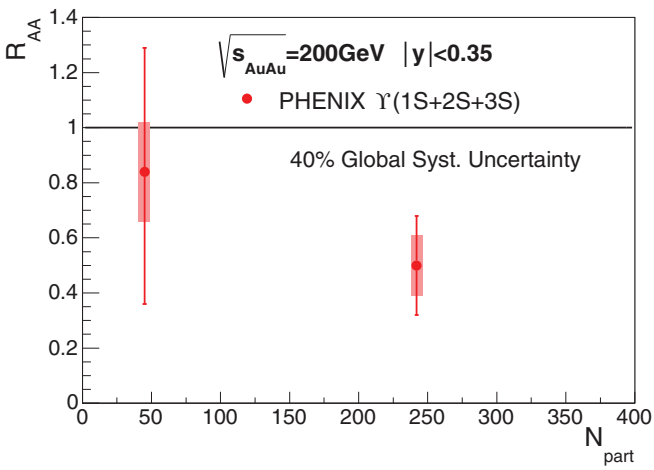

FIG. 13. (Color online) Nuclear modification factor for centrality binned data plotted as a function of N_{part}.

TABLE VII. $\Upsilon(1S + 2S + 3S)$ R_{AA} expected when the excited states are completed suppressed in Au + Au collisions along with the measured result in the 30% most central collision regime. Estimations based on Tables I and II.

	R_{AA}
No $2S$ or $3S$	0.65 ± 0.11
No $2S$, $3S$, or χ_B	0.37 ± 0.09
Measured	$0.50 \pm 0.18(\text{stat}) \pm 0.11(\text{syst}) \pm 0.19(\text{global})$

If the $\Upsilon(1S + 2S + 3S)$ yield for Au + Au collisions is equal to the yield for $p + p$ collisions times the number of binary collisions in Au + Au collisions, then $R_{AA} = 1$ and there are no nuclear modification effects. Figure 13 shows the R_{AA} as a function of the number of participants for the two centrality-split classes. The inclusive Υ states are suppressed in central 200-GeV Au + Au collisions, corresponding to large N_{part}. However, the degree of suppression in semiperipheral collisions is unclear, owing to limited statistics.

In most central events, the suppression is comparable to what is observed in $p(d) + A$ collisions [46,51–53]. Based on the lattice calculations discussed before, the bottomonia excited states should be completely dissociated in the core of Au + Au collisions at RHIC. Table VII summarizes what would be the R_{AA} observed in this study in case the only nuclear-matter effect observed is the complete suppression of these excited states. The estimation is based on the composition of the Υ states measured and the decays to the $\Upsilon(1S)$ reported in Tables I and II. The R_{AA} obtained in this analysis is consistent with the suppression of excited states if other initial- and final-state effects are ignored.

The result presented in this work agrees with that of the STAR experiment at the same energy [54]. The CMS experiment reported centrality-dependent nuclear modification factors for the separated $\Upsilon(1S)$ and $\Upsilon(2S)$ states at $\sqrt{s_{NN}} = 2.76$ TeV in Pb + Pb collisions at the LHC [55]. CMS also reported an upper limit of $R_{AA}[\Upsilon(3S)]$ of 0.10 at the 95% confidence level. Figure 14 compares the observed inclusive

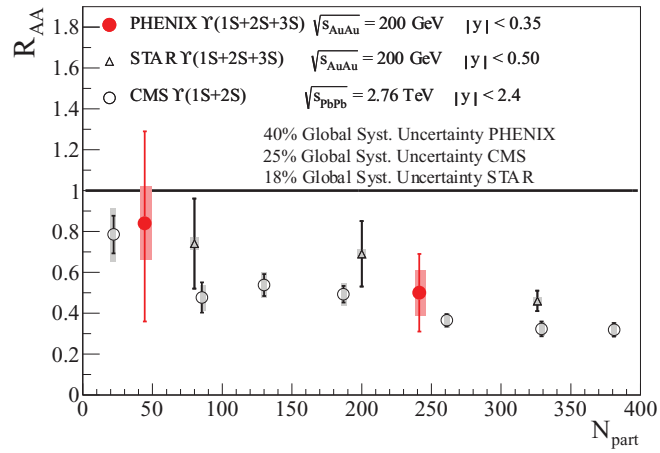

FIG. 14. (Color online) Nuclear modification factor for centrality binned data plotted as a function of N_{part} compared to STAR [54] and CMS results.

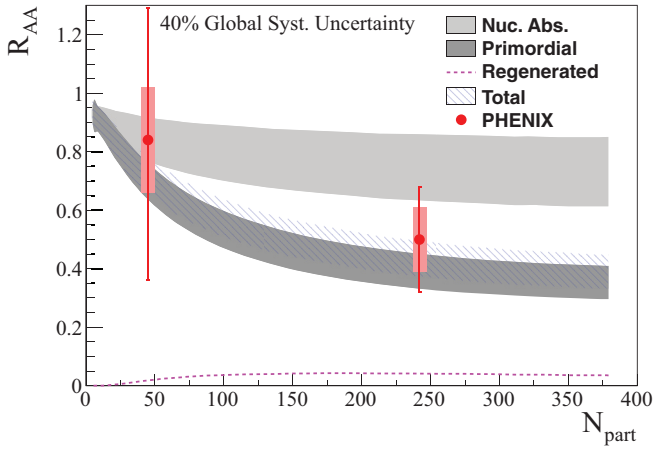

FIG. 15. (Color online) A comparison of PHENIX data to the model from Ref. [74] for the strong binding scenario.

$\Upsilon(1S+2S+3S)$ nuclear modification factor observed by PHENIX with STAR and the inclusive $\Upsilon(1S+2S)$ measurement by CMS at higher energy, showing that the observed nuclear modification factors are very similar at the two quite different energies.

Additionally, it is important to compare the measurements to various model predictions. A model by Rapp *et al.* has frequently been used to interpret J/ψ production [74]. It uses a rate-equation approach, which accounts for both suppression from cold nuclear matter, color screening of excited states (seen in Fig. 1), and regeneration mechanisms in the QGP and hadronization phases of the evolving medium. This study looked at two scenarios. The first is the strong binding scenario where the bottomonium binding energy was not affected by the presence of the QGP, remaining at the values found in vacuum, and is shown in Fig. 15. The other is the weak binding scenario where the bottomonium bound-state energies are significantly reduced in the QGP, relative to the vacuum state, adopting the screened Cornell-potential results of Ref. [75] and is shown in Fig. 16. Our data, albeit with large statistical uncertainties, are consistent with both versions of this model.

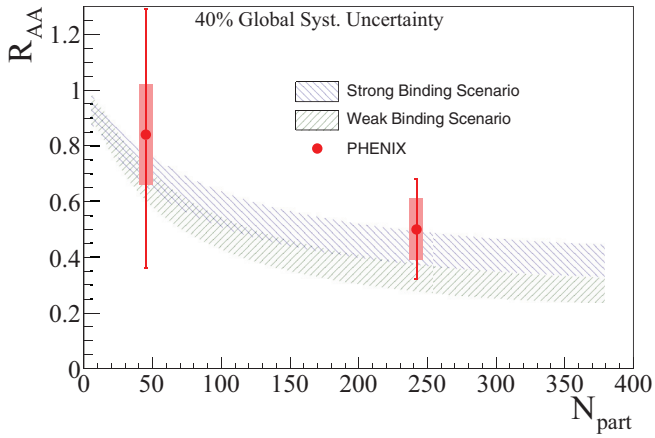

FIG. 16. (Color online) A comparison of PHENIX Υ data to the model from Ref. [74] for the weak and strong binding scenarios.

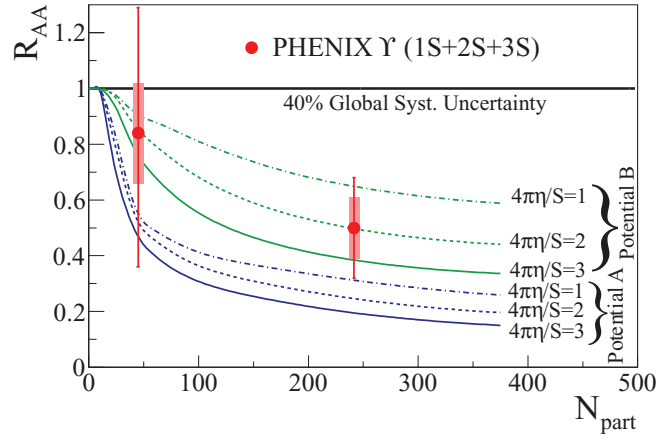

FIG. 17. (Color online) Centrality-dependent R_{AA} compared to model predictions from Strickland and Bazow [76].

More recently, two new models were suggested by Strickland and Bazow [76] based on the potential model [75], with the addition of an anisotropic momentum term. Models A and B are identical, except for an additional term in Model B, which adds an entropy contribution to the free energy. Figure 17 shows the PHENIX measurement along with the two model predictions, each with a variety of values for the ratio of the shear viscosity to the entropy density. No definitive statement can be made regarding the shear viscosity. However, the extreme potential B case appears to be favored.

V. CONCLUSIONS

In summary, we have studied the production of the sum of Υ states $1S$, $2S$, and $3S$ at $\sqrt{s_{NN}} = 200$ GeV in the midrapidity region. The dielectron channel differential cross section in $p+p$ collisions is $Bd\sigma/dy = 108 \pm 38$ (stat) ± 15 (syst) ± 11 (luminosity) pb. The nuclear modification seen in Au + Au MB collisions is 0.58 ± 0.17 (stat) ± 0.13 (syst) ± 0.23 (global), whereas it is $0.84^{+0.45}_{-0.48}$ (stat) ± 0.18 (syst) ± 0.34 (global) in the midperipheral events and 0.50 ± 0.18 (stat) ± 0.11 (syst) ± 0.20 (global) in the 30% most central events. The nuclear modification is consistent with the complete suppression of the bottomonium excited states [$\Upsilon(2S)$, $\Upsilon(3S)$, and χ_B], in qualitative agreement with most calculations as compiled in Fig. 1, assuming no cold nuclear-matter effects. There are several detailed model calculations that show good agreement with our measured modifications. The nuclear modification factors measured by PHENIX are similar to measurements by STAR at the same energy and by CMS at much higher energy, $\sqrt{s_{\rm NN}} = 2.76$ TeV.

ACKNOWLEDGMENTS

We thank the staff of the Collider-Accelerator and Physics Departments at Brookhaven National Laboratory and the staff of the other PHENIX participating institutions for their vital contributions. We acknowledge support from the Office of Nuclear Physics in the Office of Science of the Department of Energy, the National Science Foundation, a sponsored

research grant from Renaissance Technologies LLC, Abilene Christian University Research Council, Research Foundation of SUNY, and Dean of the College of Arts and Sciences, Vanderbilt University (USA); Ministry of Education, Culture, Sports, Science, and Technology and the Japan Society for the Promotion of Science (Japan); Conselho Nacional de Desenvolvimento Científico e Tecnológico and Fundação de Amparo à Pesquisa do Estado de São Paulo (Brazil); Natural Science Foundation of China (People's Republic of China); Croatian Science Foundation and Ministry of Science, Education, and Sports (Croatia); Ministry of Education, Youth and Sports (Czech Republic); Centre National de la Recherche Scientifique, Commissariat à l'Énergie Atomique, and Institut National de Physique Nucléaire et de Physique des Particules (France); Bundesministerium für Bildung und Forschung, Deutscher Akademischer Austausch Dienst, and Alexander von Humboldt Stiftung (Germany); Hungarian National Science Fund, OTKA, and the Hungarian American Enterprise Scholarship Fund (Hungary); Department of Atomic Energy and Department of Science and Technology (India); Israel Science Foundation (Israel); National Research Foundation and WCU program of the Ministry Education Science and Technology (Korea); Physics Department, Lahore University of Management Sciences (Pakistan); Ministry of Education and Science, Russian Academy of Sciences, Russian Academy of Sciences (Russia); VR and Wallenberg Foundation (Sweden); the U.S. Civilian Research and Development Foundation for the Independent States of the Former Soviet Union; the U.S.-Hungarian Fulbright Foundation for Educational Exchange; and the U.S.-Israel Binational Science Foundation.

[1] E. Eichten, K. Gottfried, T. Kinoshita, K. D. Lane, and T. M. Yan, Charmonium: Comparison with experiment, Phys. Rev. D **21**, 203 (1980).

[2] K. Adcox *et al.* (PHENIX Collaboration), Formation of dense partonic matter in relativistic nucleus-nucleus collisions at RHIC: Experimental evaluation by the PHENIX Collaboration, Nucl. Phys. A **757**, 184 (2005).

[3] T. Matsui and H. Satz, J/ψ suppression by quark-gluon plasma formation, Phys. Lett. B **178**, 416 (1986).

[4] K. Suzuki, P. Gubler, K. Morita, and M. Oka, Thermal modification of bottomonium spectra from QCD sum rules with the maximum entropy method, Nucl. Phys. A **897**, 28 (2013).

[5] T. Umeda, R. Katayama, O. Miyamura, and H. Matsufuru, Study of charmonia near the deconfining transition on an anisotropic lattice with O(a) improved quark action, Int. J. Mod. Phys. A **16**, 2215 (2001).

[6] M. Asakawa and T. Hatsuda, J/ψ and η_c in the Deconfined Plasma from Lattice QCD, Phys. Rev. Lett. **92**, 012001 (2004).

[7] S. Datta, F. Karsch, P. Petreczky, and I. Wetzorke, Behavior of charmonium systems after deconfinement, Phys. Rev. D **69**, 094507 (2004).

[8] A. Jakovac, P. Petreczky, K. Petrov, and A. Velytsky, Quarkonium correlators and spectral functions at zero and finite temperature, Phys. Rev. D **75**, 014506 (2007).

[9] G. Aarts, C. Allton, M. B. Oktay, M. Peardon, and J.-I. Skullerud, Charmonium at high temperature in two-flavor QCD, Phys. Rev. D **76**, 094513 (2007).

[10] A. Rothkopf, T. Hatsuda, and S. Sasaki, Complex Heavy-Quark Potential at Finite Temperature from Lattice QCD, Phys. Rev. Lett. **108**, 162001 (2012).

[11] G. Aarts, C. Allton, S. Kim, M. P. Lombardo, M. B. Oktay, S. M. Ryan, D. K. Sinclair, and J.-I. Skullerud (FASTSUM Collaboration), What happens to the Υ and η_b in the quark-gluon plasma? Bottomonium spectral functions from lattice QCD, J. High Energy Phys. 11 (2011) 103.

[12] G. Aarts, S. Kim, M. P. Lombardo, M. B. Oktay, S. M. Ryan, D. K. Sinclair, and J. I. Skullerud (FASTSUM Collaboration), Bottomonium above Deconfinement in Lattice Nonrelativistic QCD, Phys. Rev. Lett. **106**, 061602 (2011).

[13] G. Aarts, C. Allton, S. Kim, M. P. Lombardo, M. B. Oktay, S. M. Ryan, D. K. Sinclair, and J.-I. Skullerud (FASTSUM Collaboration), S wave bottomonium states moving in a quark-gluon plasma from lattice NRQCD, J. High Energy Phys. 03 (2013) 084.

[14] G. Aarts, C. Allton, S. Kim, M. P. Lombardo, S. M. Ryan, and J.-I. Skullerud (FASTSUM Collaboration), Melting of P wave bottomonium states in the quark-gluon plasma from lattice NRQCD, J. High Energy Phys. 12 (2013) 064.

[15] F. Karsch, E. Laermann, S. Mukherjee, and P. Petreczky, Signatures of charmonium modification in spatial correlation functions, Phys. Rev. D **85**, 114501 (2012).

[16] K. Morita and S. H. Lee, Mass Shift and Width Broadening of J/ψ in QGP from QCD Sum Rule, Phys. Rev. Lett. **100**, 022301 (2008).

[17] K. Morita and S. H. Lee, Critical behavior of charmonia across the phase transition: A QCD sum rule approach, Phys. Rev. C **77**, 064904 (2008).

[18] Y.-H. Song, S. H. Lee, and K. Morita, In-medium modification of P-wave charmonia from QCD sum rules, Phys. Rev. C **79**, 014907 (2009).

[19] K. Morita and S. H. Lee, Heavy quarkonium correlators at finite temperature: QCD sum rule approach, Phys. Rev. D **82**, 054008 (2010).

[20] P. Gubler, K. Morita, and M. Oka, Charmonium Spectra at Finite Temperature from QCD Sum Rules with the Maximum Entropy Method, Phys. Rev. Lett. **107**, 092003 (2011).

[21] Y. Kim, J.-P. Lee, and S. H. Lee, Heavy quarkonium in a holographic QCD model, Phys. Rev. D **75**, 114008 (2007).

[22] M. Fujita, K. Fukushima, T. Misumi, and M. Murata, Finite-temperature spectral function of the vector mesons in an AdS/QCD model, Phys. Rev. D **80**, 035001 (2009).

[23] J. Noronha and A. Dumitru, Thermal Width of the Υ at Large t'Hooft Coupling, Phys. Rev. Lett. **103**, 152304 (2009).

[24] H. R. Grigoryan, P. M. Hohler, and M. A. Stephanov, Towards the gravity dual of quarkonium in the strongly coupled QCD plasma, Phys. Rev. D **82**, 026005 (2010).

[25] M. Laine, A Resummed perturbative estimate for the quarkonium spectral function in hot QCD, J. High Energy Phys. 05 (2007) 028.

[26] C.-Y. Wong, Heavy quarkonia in quark-gluon plasma, Phys. Rev. C **72**, 034906 (2005).

[27] N. Brambilla, J. Ghiglieri, A. Vairo, and P. Petreczky, Static quark-antiquark pairs at finite temperature, Phys. Rev. D **78**, 014017 (2008).

[28] S. Digal, O. Kaczmarek, F. Karsch, and H. Satz, Heavy quark interactions in finite temperature QCD, Eur. Phys. J. C **43**, 71 (2005).

[29] W. M. Alberico, A. Beraudo, A. De Pace, and A. Molinari, Heavy quark bound states above T_c, Phys. Rev. D **72**, 114011 (2005).

[30] A. Mocsy and P. Petreczky, Can quarkonia survive deconfinement? Phys. Rev. D **77**, 014501 (2008).

[31] A. Mocsy and P. Petreczky, Color Screening Melts Quarkonium, Phys. Rev. Lett. **99**, 211602 (2007).

[32] P. Petreczky, C. Miao, and A. Mocsy, Quarkonium spectral functions with complex potential, Nucl. Phys. A **855**, 125 (2011).

[33] D. Cabrera and R. Rapp, T-matrix approach to quarkonium correlation functions in the QGP, Phys. Rev. D **76**, 114506 (2007).

[34] F. Riek and R. Rapp, Quarkonia and heavy-quark relaxation times in the quark-gluon plasma, Phys. Rev. C **82**, 035201 (2010).

[35] F. Riek and R. Rapp, Selfconsistent evaluation of charm and charmonium in the quark-gluon plasma, New J. Phys. **13**, 045007 (2011).

[36] A. Adare *et al.* (PHENIX Collaboration), Detailed measurement of the e^+e^- pair continuum in $p+p$ and Au + Au collisions at $\sqrt{s_{NN}} = 200$ GeV and implications for direct photon production, Phys. Rev. C **81**, 034911 (2010).

[37] A. Adare *et al.* (PHENIX Collaboration), J/ψ Production versus Centrality, Transverse Momentum, and Rapidity in Au + Au Collisions at $s_{NN} = 200$ GeV, Phys. Rev. Lett. **98**, 232301 (2007).

[38] A. Adare *et al.* (PHENIX Collaboration), J/ψ suppression at forward rapidity in Au + Au collisions at $\sqrt{s_{NN}} = 200$ GeV, Phys. Rev. C **84**, 054912 (2011).

[39] A. Adare *et al.* (PHENIX Collaboration), Ground and excited state charmonium production in $p+p$ collisions at $\sqrt{s} = 200$ GeV, Phys. Rev. D **85**, 092004 (2012).

[40] A. Adare *et al.* (PHENIX Collaboration), Cold Nuclear Matter Effects on J/ψ Yields as a Function of Rapidity and Nuclear Geometry in $d+A$ Collisions at $\sqrt{s_{NN}} = 200$ GeV, Phys. Rev. Lett. **107**, 142301 (2011).

[41] A. Adare *et al.* (PHENIX Collaboration), Transverse-momentum dependence of the J/ψ nuclear modification in d + Au collisions at $\sqrt{s_{NN}} = 200$ GeV, Phys. Rev. C **87**, 034904 (2013).

[42] A. Adare *et al.* (PHENIX Collaboration), Measurement of High-p_T Single Electrons from Heavy-Flavor Decays in $p+p$ Collisions at $\sqrt{s} = 200$ GeV, Phys. Rev. Lett. **97**, 252002 (2006).

[43] R. L. Thews, M. Schroedter, and J. Rafelski, Enhanced J/ψ production in deconfined quark matter, Phys. Rev. C **63**, 054905 (2001).

[44] A. Adare *et al.* (PHENIX Collaboration), Measurement of Bottom versus Charm as a Function of Transverse Momentum with Electron-Hadron Correlations in $p+p$ Collisions at $\sqrt{s} = 200$ GeV, Phys. Rev. Lett. **103**, 082002 (2009).

[45] J. Beringer *et al.* (Particle Data Group), Review of particle physics (RPP), Phys. Rev. D **86**, 010001 (2012).

[46] L. Y. Zhu *et al.* (FNAL E866/NuSea Collaboration), Measurement of Υ Production for $p+p$ and $p+d$ Interactions at 800 GeV/c, Phys. Rev. Lett. **100**, 062301 (2008).

[47] F. Abe *et al.* (CDF Collaboration), Υ Production in $p\overline{p}$ Collisions at $\sqrt{s} = 1.8$ TeV, Phys. Rev. Lett. **75**, 4358 (1995).

[48] R. Aaij *et al.* (LHCb Collaboration), Measurement of upsilon production in pp collisions at $\sqrt{s} = 7$ TeV, Eur. Phys. J. C **72**, 2025 (2012).

[49] V. Khachatryan *et al.* (CMS Collaboration), Measurement of the inclusive Υ production cross section in pp collisions at $\sqrt{s} = 7$ TeV, Phys. Rev. D **83**, 112004 (2011).

[50] T. Affolder *et al.* (CDF Collaboration), Production of $\Upsilon(1S)$ Mesons from χ_b Decays in $p\overline{p}$ Collisions at $\sqrt{s} = 1.8$ TeV, Phys. Rev. Lett. **84**, 2094 (2000).

[51] D. M. Alde *et al.*, Nuclear Dependence of the Production of Υ Resonances at 800 GeV, Phys. Rev. Lett. **66**, 2285 (1991).

[52] G. Moreno *et al.*, Dimuon production in proton-copper collisions at $\sqrt{s} = 38.8$ GeV, Phys. Rev. D **43**, 2815 (1991).

[53] A. Adare *et al.* (PHENIX Collaboration), $\Upsilon(1S+2S+3S)$ production in d + Au and $p+p$ collisions at $\sqrt{s_{NN}} = 200$ GeV and cold-nuclear-matter effects, Phys. Rev. C **87**, 044909 (2013).

[54] L. Adamczyk *et al.* (STAR Collaboration), Suppression of Υ production in d + Au and Au + Au collisions at $\sqrt{s_{NN}} = 200$ Gev, Phys. Lett. B **735**, 127 (2014).

[55] S. Chatrchyan *et al.* (CMS Collaboration), Observation of Sequential Υ Suppression in PbPb Collisions, Phys. Rev. Lett. **109**, 222301 (2012).

[56] K. Adcox *et al.* (PHENIX Collaboration), PHENIX central arm tracking detectors, Nucl. Instrum. Methods Phys. Res., Sect. A **499**, 489 (2003).

[57] J. Kubar, M. Le Bellac, J. L. Meunier, and G. Plaut, QCD Corrections to the Drell-Yan mechanism and the pion structure function, Nucl. Phys. B **175**, 251 (1980).

[58] J. C. Webb *et al.* (NuSea Collaboration), Absolute Drell-Yan dimuon cross-sections in 800 GeV/c pp and pd collisions, arXiv:hep-ex/0302019.

[59] T. Affolder *et al.* (CDF Collaboration), Measurement of $d\sigma/dy$ for high mass Drell-Yan e^+e^- pairs from $p\overline{p}$ collisions at $\sqrt{s} = 1.8$ TeV, Phys. Rev. D **63**, 011101 (2000).

[60] GEANT 3.2.1, GEANT 3.2.1, CERN Program Library (1993), http://wwwasdoc.web.cern.ch/wwwasdoc/pdfdir/geant.pdf

[61] T. Sjostrand, S. Mrenna, and P. Skands, PYTHIA 6.4 physics and manual, J. High Energy Phys. 05 (2006) 026.

[62] R. E. Nelson, R. Vogt, and A. D. Frawley, Narrowing the uncertainty on the total charm cross section and its effect on the J/ψ cross section, Phys. Rev. C **87**, 014908 (2013).

[63] S. S. Adler *et al.*, Midrapidity Neutral-Pion Production in Proton-Proton Collisions at $\sqrt{s} = 200$ GeV, Phys. Rev. Lett. **91**, 241803 (2003).

[64] A. Adare *et al.* (PHENIX Collaboration), Heavy quark production in $p+p$ and energy loss and flow of heavy quarks in Au + Au collisions at $\sqrt{s_{NN}} = 200$ GeV, Phys. Rev. C **84**, 044905 (2011).

[65] J. K. Yoh *et al.*, Study of Scaling in Hadronic Production of Dimuons, Phys. Rev. Lett. **41**, 684 (1978).

[66] K. Ueno *et al.*, Evidence for the Υ'' and a Search for New Narrow Resonances, Phys. Rev. Lett. **42**, 486 (1979).

[67] S. Childress *et al.*, Production Dynamics of the Υ in Proton-Nucleon Interactions, Phys. Rev. Lett. **55**, 1962 (1985).

[68] T. Yoshida *et al.*, High-resolution measurement of massive-dielectron production in 800-GeV proton-beryllium collisions, Phys. Rev. D **39**, 3516 (1989).

[69] C. Kourkoumelis, L. Resvanis, T. A. Filippas, E. Fokitis, A. M. Cnops *et al.*, Characteristics of J/ψ and Υ production at the CERN intersecting storage rings, Phys. Lett. B **91**, 481 (1980).

[70] A. L. S. Angelis *et al.* (CERN-Columbia-Oxford-Rockefeller Collaboration, CCOR Collaboration), A measurement of the production of massive e^+e^- pairs in proton proton collisions at $\sqrt{s} = 62.4$ GeV, Phys. Lett. B **87**, 398 (1979).

[71] C. Albajar *et al.* (UA1 Collaboration), Beauty production at the CERN proton-antiproton collider, Phys. Lett. B **186**, 237 (1987).

[72] D. Acosta *et al.* (CDF Collaboration), Υ production and polarization in $p\bar{p}$ collisions at $\sqrt{s} = 1.8$ TeV, Phys. Rev. Lett. **88**, 161802 (2002).

[73] M. L. Miller, K. Reygers, S. J. Sanders, and P. Steinberg, Glauber Modeling in High-Energy Nuclear Collisions, Annu. Rev. Nucl. Part. Sci. **57**, 205 (2007).

[74] A. Emerick, X. Zhao, and R. Rapp, Bottomonia in the quark-gluon plasma and their production at RHIC and LHC, Eur. Phys. J. A **48**, 72 (2012).

[75] F. Karsch, M. T. Mehr, and H. Satz, Color Screening and deconfinement for bound states of heavy quarks, Z. Phys. C **37**, 617 (1988).

[76] M. Strickland and D. Bazow, Thermal bottomonium suppression at RHIC and LHC, Nucl. Phys. A **879**, 25 (2012).